Fragility Functions for Local Failure Mechanisms in Unreinforced Masonry Buildings

Marco Nale (marco.nale@unife.it)
University of Ferrara: Universita degli Studi di Ferrara https://orcid.org/0000-0003-4565-3489
Fabio Minghini
University of Ferrara: Universita degli Studi di Ferrara
Andrea Chiozzi
University of Ferrara: Universita degli Studi di Ferrara
Antonio Tralli
University of Ferrara: Universita degli Studi di Ferrara

Research Article

Keywords: unreinforced masonry buildings, fragility functions, out-of-plane failure, local collapse mechanisms

Posted Date: March 3rd, 2021

DOI: https://doi.org/10.21203/rs.3.rs-263582/v1

Fragility functions for local failure mechanisms in unreinforced masonry buildings

Marco Nale[a], Fabio Minghini[a], Andrea Chiozzi[a], Antonio Tralli[a]

[a] Department of Engineering, University of Ferrara, Via Saragat 1, Ferrara, Italy

Abstract

The unreinforced masonry buildings can be present frequent local failure mechanisms and represent a serious life-safety hazard as recent strong earthquakes have shown. Compared to new building, existing unreinforced masonry buildings prone to be more vulnerable, not only because they have been designed without seismic or limited loading requirements, but also because horizontal structures and connections amid the walls are not always suitable. Out-of-plane collapse can be caused by important slenderness of walls also when connections are effective.

The purpose of this paper is to evaluate fragility functions for unreinforced masonry walls in the presence of local failure mechanisms considering the out-of-plane response. The wall response, very often, can be idealized as rigid bodies undergoing rocking motion. Depending on its configuration, a wall is assumed either as a rigid body undergoing simple one-sided rocking or an assembly of two coupled rigid bodies rocking along their common edge. A set of 44 ground motions from earthquake events occurred from 1972 to 2017 in Italy is used in this study. The likelihood of collapse is calculated via Multiple Stripe Analysis (MSA) from a given wall undergoing a specific ground motion. Later, the single fragility functions are suitably combined to define a typological fragility function for a class of buildings. The procedure is applied to a historical aggregate in the city center of Ferrara (Italy) as a case study. The fragility functions developed in this research can be a very helpful tool for estimating damage and economic loss for unreinforced masonry buildings and for a seismic assessment on a regional scale.

Keywords: unreinforced masonry buildings, fragility functions, out-of-plane failure, local collapse mechanisms

1. INTRODUCTION

UnReinforced Masonry (URM) buildings represent a large part of the Italian building stock. Compared to new buildings, existing URM buildings tend to be even more vulnerable to earthquakes. In Italian historical centers, this is essentially due to the following causes.

1) Old buildings may have been strongly altered over time, often resulting in a reduction of cross-section areas of masonry walls, a general weakening of mutual connections between walls and floors, and sometimes a significant increase in the seismic masses.
2) Materials may be seriously degraded due to weathering, rising damp, and poor maintenance.
3) In some territories, such as a large part of the Po River plain, seismic design has become mandatory only since 2005, and most of the buildings have been designed in the absence of specific provisions for earthquake resistance.

Recent seismic events (Decanini et al. 2004; Indirli et al. 2013; Penna et al. 2014; Sorrentino et al. 2019) have provided evidence that Out-Of-Plane (OOP) collapse mechanisms in URM structures still represent a serious life-safety hazard. In fact, under seismic actions, existing URM buildings are often subjected to local collapse mechanisms involving partial or whole OOP failure of façade walls. Both activation and evolution up to collapse of these mechanisms strictly depend on stiffness and strength of connections between facade walls and other structural elements such as partition walls, floors and roof.

In Italy, the seismic analysis of historical URM buildings based on the assessment of collapse mechanisms starts with Giuffrè (1996). Kinematic limit analysis is considered one of the most reliable tools to assess OOP failure of masonry walls, and is currently adopted by Italian building code (Ministero delle Infrastrutture e dei Trasporti 2018). This analysis method is based on the following steps:

1) use of the kinematic theorem of limit analysis to select, among various OOP mechanisms, that leading to the minimum seismic load multiplier;

2) imposition, for the selected mechanism, of equilibrium conditions corresponding to a generic, deformed configuration;
3) evaluation of the capacity curve for the mechanism as a continuous function of the horizontal displacement of a control point;
4) transformation of the capacity curve for the mechanism into the capacity curve corresponding to an equivalent Single Degree-Of-Freedom (SDOF) system;
5) location, on the SDOF curve, of a limiting displacement corresponding to the considered limit state and comparison with the displacement demand.

Various authors showed the drawbacks related with the use of such an approach, which often underestimates the actual resources of URM walls (Shawa et al. 2012; Giresini et al. 2015; Sorrentino et al. 2016).

A more performing approach appears to be the nonlinear dynamic analysis of the walls considered as rigid rocking blocks. The study of rocking oscillators began with the seminal paper by Housner (1963), that derived a SDOF equation of motion for the out-of-plane response of a parapet wall (PW). Following that study, the research focused on the description of the dynamic response of rocking blocks subjected to either earthquake excitations or pulse (Yim et al. 1980; Spanos and Koh 1984). It has been found that this response may be characterized by dynamic instability and strong nonlinearity. Later, other models were adopted introducing equivalent SDOF models to govern the dynamic behavior of complex multi-block rocking systems (Sorrentino et al. 2008; DeJong and Dimitrakopoulos 2014). A SDOF force-displacement idealization of the rocking behavior of URM walls was proposed by Doherty et al. (2002).

A unified, probabilistic approach taking account of uncertainties, vulnerability, and risk can provide, with the use of nonlinear dynamic analysis, a better estimate of structural safety levels. One of the main tools in PEER - PBEE framework is the fragility function (Deierlein et al. 2003; Krawinkler and Miranda 2004). For the rocking block, various studies provided fragility functions in terms of

different intensity measures (Dimitrakopoulos and Paraskeva 2015; Lagomarsino 2015; Chiozzi et al. 2017). The methods available in the literature to derive fragility functions can be divided into four categories (Pitilakis et al. 2014; Silva et al. 2019): analytical, empirical, expert judgment, and hybrid. Fragility functions have also been proposed to describe the global behavior of masonry structures (Lagomarsino and Giovinazzi 2006; Rota et al. 2010; Spillatura et al. 2014). Most of these researches consider only the in-plane response of masonry walls. More recent studies propose fragility functions for OOP mechanisms based on kinematic limit analysis (Zuccaro et al. 2017). Simões et al. (2019a, b, 2020) developed fragility functions for URM buildings combining in- and out-of-plane wall responses. In particular, for the OOP response, nonlinear kinematic analyses are used.

This paper presents a procedure to derive fragility functions for OOP mechanisms in URM buildings based on nonlinear dynamic analysis. A rigid block model is adopted for load-bearing walls. Fragility functions are derived considering the uncertainties associated with the peculiarities of masonry structures. These uncertainties are both aleatory and epistemic. The aleatory variables involved, such as wall geometry, masonry mass density, loads transferred from floors and roof, are treated by the Monte Carlo method (Zio 2013). Epistemic uncertainty is treated through the use of logical trees (Simões et al. 2019b). In the end, the individual fragility functions obtained are combined to define a typological fragility function for a class of masonry buildings. The approach adopted for the derivation of fragility functions is described in detail in the following sections. The method is then applied to a case study concerning a historical aggregate in the city center of Ferrara (Italy). This historical aggregate was studied in Nale et al. (2020) where some preliminary results have been exposed.

2. BUILDINGS DATABASE

2.1. Cartis database

The Cartis database (Zuccaro et al. 2016) is an inventory of buildings typologies on regional scale funded by the Italian National Civil Protection Department and elaborated by ReLUIS (Rete dei

Laboratori Universitari di Ingegneria Sismica e Strutturale). The data collection is based on an interview, which consists of filling out a form on a city, divided into compartments. For each compartment, a technician (i.e. engineers, architects) collects the relevant information on the relevant types of buildings (e.g. age of structures, type of structures, geometrical data, etc.). This information is more detailed than available standard methods (ISTAT data, Census Database) and can more effectively support to the creation of vulnerability models. In this paper, this database is used to create typological fragility functions for local failure mechanisms in unreinforced masonry structures.

2.2. Case study

The historic center of Ferrara is made up of 92% masonry buildings and the remainder is made up of reinforced concrete and mixed structures. The structures are mainly by less than 3 stories for 83%, albeit unevenly distributed concerning the construction periods of the city from the 14th to the 19th century (Dolce et al. 2015). In addition to the data extrapolated from the Cartis database, it was decided to survey a historical aggregate of buildings in the center of Ferrara to improve the knowledge of masonry buildings. Table 1 shows the main parameters of the buildings in the historic center of Ferrara from Cartis Database.

For the selected compartment there are two typologies of buildings present in the city center of Ferrara (MUR 1 and MUR 2) (Figure 1). The MUR1 typology refers to buildings from two to four stories, belonging to the oldest part of the historic center (medieval area) but also to the Renaissance area up to the 1800s and early 1900s (Figure 2). The MUR2 typology is more recent (from 1920 to 1945) and has a different percentage of tie rods on the total of the buildings, even though it also has a wooden floor and a wooden roof. The buildings of these types are for residential, commercial, tourist-accommodation, and office use (Figure 3). The structural behavior of URM buildings is directly dependent on the materials and constructive details and indirectly dependent on the usage and state of conservation. One of the main challenges when assessing existing buildings is the definition of the mechanical properties of the materials (e.g. quality of clay brick wall see Figure 4). In general, the

weakest points of URM buildings are the poor connections (between walls or between walls and floors or roof) and the limited stiffness of timber floors (Figure 5).

3. SEISMIC ASSESSMENT

3.1. Description of the approach

For the seismic assessment, the local response is related to the activation of out-of-plane collapse mechanisms of parts of the buildings insufficiently connected to the rest of the structure. Furthermore, fragility curves were used to describe the local response in the probabilistic context. These curves are useful for defining related vulnerability models. The intensity measure (IM) adopted in this work is the peak ground acceleration (PGA) as required by Italian building code (Ministero delle Infrastrutture e dei Trasporti 2018) and which represents a common choice in the case of URM buildings. Epistemic uncertainty was treated using a logic tree approach that allows describing the vulnerability of each mechanism (Section 4.1). The aleatory uncertainty of each mechanism deriving from the properties of the materials, the geometry of the elements, and the loads applied on the mechanism have been treated with the Monte Carlo method (Section 4.2). The input parameters for a given mechanism were treated as one of the possible combinations of existing walls. To create a group of walls representative of the type of structures considered, a number of 1000 walls have been created. Such walls are the final result of all the uncertainties considered deriving from the epistemic and aleatory ones.

To create the topological fragility curves we proceeded as follows:

- identification of all possible configurations of the collapse mechanisms and relative weights (Section 4.1)
- extrapolation of the main collapse mechanisms from the logic tree (Section 4.1)
- generation of walls for the various mechanisms (Section 4.2)
- multiple stripe analysis and creation of fragility curves (Paragraph 5.2.4)
- typological fragility curves by combining the weights of mechanisms (Section 5.3)

3.2. Comparison between the Italian code and non-linear dynamic analysis

In this section, a critical review of seismic response assessment techniques for local collapse mechanisms in existing masonry structures is discussed. To have statistically robust results, three type of walls with the two different configurations of constraints are subjected to non-linear dynamic analyses (Table 2). Each wall was subjected to 44 accelerograms with 2 constraint configurations for 10 different amplitude scale of ground motion. A total of 1320 non-linear dynamic analyses were performed. The results of the dynamic analysis are expressed by the ratio between energy demand (E_D) and capacity (E_C) (Shawa et al. 2012; Sorrentino et al. 2016). The energy demand (E_D) is calculated as the maximum potential energy during the seismic action or as the sum of the potential and kinetic energy at instability. The capacity energy (E_C) is calculated as the difference in the potential energy of the system. In Figure 7, the results obtained from the non-linear dynamic analysis are compared with the methods proposed by the Italian code (Ministero delle Infrastrutture e dei Trasporti 2018, 2019). In the Italian code, the evaluation of local collapse mechanisms is recommended with two approaches: the force-based approach and the displacement-based approach. The force-based approach defines the acceleration capacity (a_0^*). The relative acceleration demand is the peak ground acceleration (PGA) divided by behavior factor q = 2.0. The ratio between demand acceleration and capacity acceleration is used to compare the force-based approach to a dynamic approach. The displacement-based approach, on the other hand, defines a displacement capacity (d_u^*). The corresponding demand displacement is evaluated using the spectral displacement ($S_{De}(T_S)$) at the secant period (T_S) of the local mechanism. The ratio between demand and capacity is used to compare the displacement-based approach to the dynamic approach. As it can be observed in Figure 7, the number of non-conservative cases is less for the one-sided mechanism, while it increases in the case of two-blocks mechanism. Furthermore, it is possible to see how displacement-based approach can reduce the number of non-conservative cases. Both approaches confirm that they are less conservative

than non-linear dynamic analyses. This evidence is due to several factors, for more details see (Shawa et al. 2012; Mauro et al. 2015; Sorrentino et al. 2016).

3.3. Dynamic analysis of local collapse mechanisms

Modeling unreinforced masonry walls, subjected to seismic loads, represents an important challenge, from both engineers and researchers because of its complexity of being described with nonlinear dynamic analysis. In this study, a single degree of freedom (SDOF) numerical model is used for the analysis of their dynamic behavior under seismic action.

3.3.1. Modeling strategy

The equation of motion for rocking block associated with a given local mechanism can be derived using Lagrange's equation:

$$\frac{d}{dt}\left(\frac{\partial T\left(\phi,\dot{\phi}\right)}{\partial \dot{\phi}}\right)-\frac{\partial T\left(\phi,\dot{\phi}\right)}{\partial \dot{\phi}}+\frac{\partial V\left(\phi\right)}{\partial \dot{\phi}}=-B\left(\phi\right)\ddot{u}_g+Q\left(\phi\right) \tag{1}$$

where T is the kinetic energy, V potential energy, $-B\left(\phi\right)\ddot{u}_g$ is the generalized inertial force induced by earthquake excitation and Q the generalized force provided by static forces and ϕ is the lagrangian parameter that describes the motion. Equation 1 can be written in the following form:

$$I\left(\phi\right)\ddot{\phi}+J\left(\phi\right)\dot{\phi}+G\left(\phi\right)=-B\left(\phi\right)\ddot{u}_g+Q\left(\phi\right) \tag{2}$$

where $I\left(\phi\right), J\left(\phi\right), G\left(\phi\right)$ and $B\left(\phi\right)$ are non-linear functions of ϕ. It is also possibly derived from Eq 2 for different local mechanisms, the static load multiplier that activates the mechanism, assuming in the resting position null acceleration and velocity ($\ddot{\phi}=0,\ \dot{\phi}=0,\ \phi=0$), we obtain:

$$\lambda=-\frac{Q\big|_{\phi=0}-G\big|_{\phi=0}}{g\,B\big|_{\phi=0}} \tag{3}$$

where g is the gravity acceleration. The same load multiplier can be obtained by the limit analysis approach. In rocking systems, the energy dissipation is associated with the impact of the blocks (Housner 1963; Yim et al. 1980; Spanos and Koh 1984). The restitution coefficient is defined, indeed, as the ratio of angular velocity after and before the n^{th} impact.

3.3.2. One-sided rocking

A one-sided rocking can be assumed for a wall even though the presence of internal constraints such as transverse walls and horizontal structural elements. The equation of one-sided rocking can be written similarly to the equation on the two-sided rocking rigid body:

$$I_0\ddot{\phi} + gM_bR\sin(\alpha-\phi) = -M_bR\ddot{u}_g\cos(\alpha-\phi) \tag{4}$$

where I_0 is the polar moment of inertia with the pivot point 0, M_b is the mass of the block and α is the internal angle and R is the length of the half-diagonal. In the case of vertical restraint, the rotation ϕ of the system remain positive (Figure 8). For one-sided cases, experimental evidence shows that energy dissipation depends on the interface between the constraint and the block (Sorrentino et al. 2011).

$$\eta_{1s} = \left(1-\frac{3}{2}\sin^2\alpha\right)^2\left(1-\frac{3}{2}\cos^2\alpha\right) \tag{5}$$

For better and more accurate modeling of the seismic behavior of the wall, a tri-linear moment-curvature relationship with a finite initial stiffness can be assumed on the basis of experimental test (Doherty et al. 2002). The tri-linear function takes into account initial imperfections, non-linear material behavior, and the second-order effects. If this configuration is assumed with the tri-linear moment-rotation relationship, the motion equations can be written as follows (Boscato et al. 2014):

$$
\begin{aligned}
\ddot{\phi} &= -\frac{WR}{I_0}\left[\frac{k_i}{WR}\phi + \frac{\ddot{x}_g(t)}{g}\cos\left(\alpha - |\phi|\right)\right] && \text{if } |\phi| \le \alpha_1 \\
\ddot{\phi} &= -\frac{WR}{I_0}\left[\operatorname{sgn}\left(\phi\right)\frac{k_i}{WR}\alpha_1 + \frac{\ddot{x}_g(t)}{g}\cos\left(\alpha - |\phi|\right)\right] && \text{if } \alpha_1 < |\phi| \le \alpha_2 \\
\ddot{\phi} &= -\frac{WR}{I_0}\left[\operatorname{sgn}(\phi)\frac{k_f}{WR}\left(\alpha - |\phi|\right) + \frac{\ddot{x}_g(t)}{g}\cos\left(\alpha - |\phi|\right)\right] && \text{if } |\phi| > \alpha_2
\end{aligned}
\tag{6}
$$

where R is the distance of the center of gravity from the rotation pivot, k_i is the initial stiffness ($k_i = \frac{WR\sin(\alpha)}{\alpha}\cdot\frac{\alpha-\alpha_2}{\alpha_1}$); and k_f is the final stiffness $k_f = \frac{WR\sin(\alpha)}{\alpha}$ with parameter $\alpha_1 = \tan^{-1}\left(3\frac{\Delta_1}{2H}\right)$ (Table 3).

3.3.3. Two block mechanism

The two-block mechanism can be used to describe the dynamic behavior of a wall that is characterized by the formation of the classical pivot interface at the wall top, bottom, and mid-height. The top and bottom pivot can rotate if they are under a ground motion excitation. The mechanism is described by these main parameters: α_1 and α_2 the describe the slenderness of the two blocks; I_{01} and I_{02} that are the polar moment of inertia regarding the relative mass centers M_{b1} and M_{b2} that are the masses of the bottom and the top blocks (Figure 9). The resulting equation of motion is equivalent to those prosed in the literature (Sorrentino et al. 2008; DeJong and Dimitrakopoulos 2014; Mauro et al. 2015) and can be written as follows;

$$
\begin{aligned}
&\left(I_{01} + B_1 I_{02} + B_2 M_{b2} R_2^2\right)\ddot{\phi} + \left(C_1 I_{02} + C_2 M_{b2} R_2^2\right)\dot{\phi} + gAR_2\left[M_{b1} + M_{b2}\left(1 + \frac{B_2}{4A^2}\right)\right] = \\
&-A\left(M_{b1} + M_{b2}\right)R_2\cot\left(\alpha_1 - \phi\right)\ddot{x}_g + Q
\end{aligned}
\tag{7}
$$

with the following system coefficients that are not constant but are functions of rotation ϕ.

$$
\begin{aligned}
A &= \frac{\sin(\alpha_2)}{\sin(\alpha_1)}\sin\left(\alpha_1 - \phi\right) \\
B_1 &= \frac{\mathrm{A}^2\cot^2\left(\alpha_1 - \phi\right)}{1 - A^2} \\
B_2 &= 4A^2\left[1 + \sqrt{B1}\right]
\end{aligned}
\tag{8}
$$

$$C_1 = \left[1 - \frac{A^2}{\sin^2(\alpha_1 - \phi)}\right]\left(\frac{A}{1-A^2}\right)^2 \cot(\alpha_1 - \phi)$$

$$C_2 = \frac{B_2}{2}\left[\frac{A}{\sqrt{1-A^2}} - \frac{A^2-2}{(1-A^2)}\cot(\alpha_1 - \phi)\right]$$

$$Q = -2ANR_2\sqrt{B_2}\cos^2(\alpha_2)\left[\frac{1}{\sqrt{B_2}\cos^2(\alpha_2)} + 1 + \xi\tan^2(\alpha_2) + \frac{(\xi-1)\tan(\alpha_2)\sqrt{1-A^2}}{A}\right]$$

The critical rotation and the horizontal load multiplier of the system become:

$$\phi_{cr,0} = \alpha_1$$

$$\lambda = \tan(\alpha_1)\frac{M_{b1} + \left(M_{b2} + \frac{N}{g}\right)\left(2 + \frac{\tan(\alpha_2)}{\tan(\alpha_1)}\right) + (2\xi - 1)\frac{N}{g}\frac{\tan(\alpha_2)}{\tan(\alpha_1)}}{M_{b1} + M_{b2}}\dot{u} \tag{9}$$

and the coefficient of restitution η_{tb} is defined as follows:

$$\eta_{tb} = \frac{M_{b1}R_1^2 + I_{01}\frac{\tan\alpha_2}{\tan\alpha_1} - 2M_{b1}R_1^2\sin^2\alpha_1 + M_{b2}R_1^2\left[2 + \frac{\sin\alpha_1\cos\alpha_1}{\tan\alpha_2} - \sin^2\alpha_1\left(4 + \frac{\tan\alpha_2}{\tan\alpha_1}\right)\right]}{M_{b1}R_1^2 + I_{01} - I_{02}\frac{\tan\alpha_2}{\tan\alpha_1} + M_{b2}R_1^2\left[2 + \sin\alpha_1\cos\alpha_1\left(\frac{1}{\tan\alpha_2} + \tan\alpha_2\right)\right]} \tag{10}$$

The coefficient of restitution depends on the slenderness of the wall and the position of the hinge. For the stockier wall and lower intermediate hinge, the energy dissipation will decrease. For this type of mechanism, the value of the coefficient of restitution is between 0.84 and 0.90 from experimental tests (Graziotti et al. 2016). Using this model is not considered the progressive damage (Doherty et al. 2002) and no energy damping term (Tomassetti et al. 2019).

The rocking response results are obtained from a MATLAB code that numerically solves the nonlinear equations by means of a 4th-5th order Runge-Kutta integration technique (The Mathworks Inc. 2016).

4. EVALUATION OF UNCERTAINTIES

To characterize the behavior of these buildings, the main epistemic and aleatory uncertainties are briefly defined in the next sections to account for the possible variations within this class of buildings. The geometry of the building is not considered an uncertainty as the layout of the buildings is similar. Aleatory uncertainty is classified as irreducible uncertainty and refers to a property of the system associated with variability, whereas epistemic uncertainty can be reduced and it is associated with a lack of knowledge by the analyst (Beer et al. 2013).

4.1. Epistemic uncertainties

The epistemic uncertainties for the analysis of the local behavior are related to the incomplete knowledge about the structure of the buildings. These features are treated by the logic-tree approach (Simões et al. 2020). Figure 10 presents the logic-tree for the URM buildings in Ferrara for different categories of buildings (MUR1 and MUR2). The end of a branch of the tree represents a class of possible mechanisms with specific features and the final weights. The weight attributed to the class of mechanisms is determined by multiplying the weight of all the component branches of the tree. More in detail, from the first logic tree it is possible to obtain for the two main classes of masonry buildings with the relative associated weights for the various types of collapse mechanisms (Figure 11). The main mechanisms obtain from the logic tree are: overturning 1 floor, overturning 2 floor, overturning 3 floor, overturning 4 floor and vertical bending. With the expression overturning *n* floor, we mean a one-sided rocking with a height of the block corresponding to *n* floors. The relative mechanism is obtained for the sum of the weights that contain that mechanism. Only for the two-block mechanism, we consider a mechanism at the top floor of the building. The vertical bending in the lower floors have been exclude because the walls are more loaded than the top floor. This increase the stability of the wall (Mauro et al. 2015).

These weights will be used to create the typological curve for out-of-plane mechanisms.

4.2. Aleatory uncertainties

Aleatory uncertainties are related to the randomness of a certain phenomenon. For the analysis of the global behavior, the aleatory variables account for variations on the mechanical properties of masonry and geometrical properties of the wall. It is proposed to treat these aleatory variables by the Monte Carlo Method (Zio 2013) to define, in a random way, the properties to be assigned to the numerical models. The parameter ranges were chosen using the ranges extrapolated from the Cartis database and possible mechanisms. The random generation of the parameters was done considering an interval set described by a lower and higher value. Generation occurs assuming a uniform distribution. This choice was made due to the fact that the information about the parameters was vague. The possible choice of a normal or lognormal probability distribution was not compliant because there were not enough tests for the relative parameters. The walls vary with a height between 3.00 m and 12.50 m and a thickness between 0.28 and 0.43 m. The thickness was also defined considering causal values compatible with the possible combination of the bricks (i.e. single-leaf wall). A total of 1000 simulations are considered to have a sufficient number of results to reach a good convergence in the estimation. In the random generation of the walls, the variability of the loads, the percentages of openings in the walls (Figure 12) and the presence of transverse connections were considered.

5. FRAGILITY ANALYSIS

5.1. General approach

A fragility function is defined as a lognormal cumulative distribution function:

$$P\left(C\middle|IM=x\right)=\Phi\left(\frac{\ln\left(x/\theta\right)}{\beta}\right) \tag{11}$$

where $P(C|IM=x)$ is the probability that a ground motion with $IM=x$ will cause the collapse of the wall, $\Phi(\ )$ is the standard normal cumulative distribution function (CDF), θ is the mean of the fragility function and β is the standard deviation of $\ln IM$. To create a fragility curve, it is necessary to estimate

the parameters that describe the curve, in particular the mean value and the standard deviation for a lognormal cumulative distribution function. The parameters of the fragility curves can be estimated by various methods. The two most common are the incremental dynamic analysis (IDA) and multiple stripe analysis (MSA). A multi-stripe analysis (MSA) is used in this work (Figure 13).

5.2. Derivation of fragility curves

5.2.1. Selection of ground motions

In this paper, we used ground motion records from the ESM and ITACA databases (Bindi et al. 2011). The 46 ground motion records used for this study have been derived from 22 different events, recorded in different regions of the Italian territory between 1972 and 2017 (Table 4). These ground motions are within a specified range: magnitude M_w between 5.0 and 7.0, Joyner-Boore distance R_{jb} between 0 and 30 km, EC8 soil classification from B to E, and strike-slip, reverse or reverse-oblique faults. The number of ground motions is in accordance with NEHRP Guidelines (Whittaker et al. 2011). The ground motions are mainly obtained by the Italian accelerometric network (Rete Accelerometrica Nazionale, RAN) managed by the Italian Civil Protection Department (DPC) and the national seismic network managed by Istituto Nazionale di Geofisica e Vulcanologia (INGV). The selected ground motions take into account a wide range of PGA as well as PGV (Suzuki and Iervolino 2017).

5.2.2. Intensity Measure (IM)

The intensity measure is a parameter that quantifies the intensity of ground motion and serves as a connection between probabilistic seismic hazard analysis and probabilistic structural response analysis. The choice of this parameter has relevant effects on structural response. In this study, the peak ground acceleration (PGA) is selected as an intensity measure. In the Italian Building code, PGA is an index for seismic design but it has long been known that this type of intensity measure is, in general, inefficient for evaluating seismic risk (Housner 1965). For low masonry buildings, as those

presented in the case study, PGA is considered a reliable parameter (Lagomarsino and Giovinazzi 2006).

5.2.3. Engineering demand parameter (EDP)

For the correct evaluation of the fragility curve, an appropriate engineering demand parameter (EDP) is necessary for association with the damage state. In this paper, the damage state considered is the collapse damage state that corresponds to the complete overturn of the block. The absolute peak rocking rotation $|\phi_{\max}|$ divided with the slenderness α is the EDP:

$$EDP = \frac{|\phi_{\max}|}{\alpha} \tag{12}$$

The choice of this dimensionless EDP is physically explained: the large value of EDP implies that the block starts rocking (EDP >0), high values (e.g. EDP > 1.0) show overturning as a consequence of rocking (Table 5). The parameter α for the vertical bending is assumed equal to the slenderness α_1 of lower block (Sorrentino et al. 2008). The collapse is considered with a EDP =1.0. This choice is conventional. In fact, this value occurs when there is a static instability. It is possible that the block rocking without overturning with EDP>1 because the problem is strongly nonlinear (Dimitrakopoulos and Paraskeva 2015).

5.2.4. Multiple stripe analysis (MSA)

The parameter estimators were obtained using the maximum likelihood method. This method is widely used in literature as an alternative to the moments method to estimate the parameters. This method is briefly described hereinafter.

The rocking analyses are performed for a level of intensity $IM=x_j$ which will give a number of collapses over the total number of the ground motions set. The probability of having z_j collapses in n_j ground motion per fixed intensity level is expressed as follows

$$P\left(z_j \text{ collapses in } n_j \text{ ground motions}\right)=\binom{n_j}{z_j} p_j^{z_j}\left(1-p_j\right)^{n_j-z_j} \tag{13}$$

where the collapse of the block can be caused with a probability p_j for a certain level of intensity IM = x_j. The observations of non-collapse and collapse can be assumed as ground motion independent of each other. The purpose of deriving the various collapse probabilities for different intensity levels is to derive a function with the highest probability from the collapse data observed by the rocking analysis. This is possible due to the likelihood method. The likelihood for the entire set of data obtained from multiple levels of IM is expressed by the product of the binomial probabilities (equation 13) and is described as follows.

$$\text{Likelihood}=\prod_{j=1}^{m}\binom{n_j}{z_j} p_j^{z_j}\left(1-p_j\right)^{n_j-z_j} \tag{14}$$

where Π indicates the product of all *m* level of IM. The probability function is made explicit by substituting equation 13 for pj

$$\text{Likelihood}=\prod_{j=1}^{m}\binom{n_j}{z_j}\Phi\left(\frac{\ln\left(x_j/\theta\right)}{\beta}\right)^{z_j}\left(1-\Phi\left(\frac{\ln\left(x_j/\theta\right)}{\beta}\right)\right)^{n_j-z_j} \tag{15}$$

Maximizing the likelihood function, it is possible to obtain the estimator parameters of the fragility curve that can be written:

$$\left\{\hat{\theta},\hat{\beta}\right\}=\arg\max_{\theta,\beta}\sum_{j=1}^{m}\left\{\ln\binom{n_i}{z_j}+z_j\ln\Phi\left(\frac{\ln\left(x_j/\theta\right)}{\beta}\right)+\left(n_j-z_j\right)\ln\left(1-\Phi\left(\frac{\ln\left(x_j/\theta\right)}{\beta}\right)\right)\right\} \tag{16}$$

5.3. Proposed typology fragility curves

The creation of typological fragility curves allows to include all uncertainties and describe a general behavior of the structure or element. Figure 14 shows the sensitivity analysis made for the mechanism

of vertical bending. The parameters considered are the position of the formation of the hinge (Figure 14a) and the influence of the vertical force N (Figure 14b). In our case, we consider a wall 0.3×3.0 m. The position of the hinge has been changed considering the h_1 / h ratio which varies from 0.5 to 0.8 (ABK 1981; Graziotti et al. 2016). This parameter has little influence on the variation of the fragility curve. Instead, the vertical force affects the vulnerability of the wall. The vertical force was considered as the effect of the load due to the span of the slab. This force was applied in the center of the wall thickness. The type of floor chosen is a wooden slab at the roof of the structure (load of 2.5 kN/m^2). The span of the slab varies from 1 to 5 meters found in the masonry structures in Ferrara (Table 1). In Figure 14b, the span of the floor *L* varies from 0 m (where the floor does not discharge on the wall) to 5.0 m. It is possible to see how this parameter has small influence. It can be seen that the vertical force at the top is a stabilizing component for the wall, making it less vulnerable. This can also be seen with static and dynamic analyses (Mauro et al. 2015). Subsequently, the fragility curves for the various mechanisms were created by varying the parameters. Each fragility curve was obtained by carrying out 44 nonlinear dynamic analyses for 9 different levels of intensity. For each curve, 396 nonlinear dynamic analyses were carried out for each wall considered. From the data extrapolated from Cartis, intervals of parameters were obtained which were then inserted to carry out the analysis. The distributions could not be extrapolated due to the lack of information on the individual buildings. The database allows us to provide general data on a group of buildings. For each mechanism identified, a population of walls was created with randomly generated geometric parameters. This choice is the most reasonable for the availability of data. For the mechanisms, a Monte Carlo method was applied with a population of 1000 walls. From here a group of fragility curves has been obtained (Figure 15). For each group of fragility curves, it is possible to obtain its average curve (bold black curves in the figures).

In addition to the fragility curves for the various collapse mechanisms derived from the creation of a population of walls, the fragility curves for the mechanisms present in the case study were created

(Figure 16) with its average curve (bold black curves in the figures). The most significant comparison is between the average curve obtained from the population of MUR1 (this category constitutes 90% of the total of the buildings surveyed) with the curve obtained from the survey of the compartment. For completeness, the comparison between the curves of the MUR2 population with those obtained from the survey is also reported (Figure 17). The typological fragility curves MUR1 and MUR2 are very similar despite being in two different typological categories because the parameters vary not much (Table 1). Also, the buildings have good masonry qualities and textures, good transversal connections, and the presence of tie rods or tie beams. It is possible to say in general that un seismic action, buildings from different historical periods do not have great differences. From both graphs, it can be seen how the average population curve is more conservative than that obtained from the survey. This evidence is due to the greater number of walls analyzed for the various mechanisms obtained by the population than the number of walls obtained from the survey. The difference between the curves obtained is due to the level of knowledge of the walls. The survey increases the level of knowledge about the walls therefore the curve reduces the uncertainty associated with the geometry of the wall and provides a more detailed description of the walls for the historic aggregate. Moreover, the curves obtained from the survey consider the good masonry quality of the walls and the connection with the transverse walls (while in the Cartis database there is no information about it). This information allows us to have representative curves than the curves database. Transversal connections help to greater stability of the wall compared to its absence.

Figure 17 shows the overall global typological curves for out-of-plane mechanisms. These curves are obtained by weighting the mean values and variances previously obtained for the individual class of mechanisms. These weights are obtained from the logical trees created to evaluate the relative possible collapse configurations (Figure 11).

6. CONCLUSIONS

This paper presents a procedure for the derivation of fragility functions for local failure mechanisms in unreinforced masonry buildings. The proposed method starts with the data processing of the Cartis database. A qualitative description of the building stock and associated relevant uncertainties (material, geometrical, loads) are initially considered. Epistemic uncertainties are included through the use of logical trees. Mechanical models, the validity of which is documented in the literature also from results of experimental campaigns, are introduced to analyze the out-of-plane response of masonry walls. A dynamic approach is used, adopting a multiple stripe analysis method to derive punctual fragilities. Finally, fragility functions are fitted to the computed fragilities.

The method is applied to historical aggregates of URM buildings. For the selected compartment in the city center of Ferrara, two building typologies (MUR 1 and MUR 2) are identified. MUR1 typology refers to buildings belonging to the oldest part of the historic center (medieval area) but also to the Renaissance area up to the 1800s and early 1900s, whereas MUR2 typology is more recent (from 1920 to 1945) and has a different percentage of tie rods on the total of the buildings.

The final fragility functions provide an overall assessment of the seismic vulnerability for these classes of buildings. The results show the moderate quality of the building stock. However, the introduction of effective tie rods, modifying the out-of-plane failure mechanisms from rocking to vertical bending, can dramatically reduce the vulnerability of aggregates, keeping the streets of historic centers operational even after strong earthquakes.

Typological fragility curves for these local mechanisms then provide a useful tool for the evaluation of damages and the assessment of economic losses. In future research, we will analyse the influence of the interaction between the floor effect of masonry structures and the local collapse mechanisms in the evaluation of damage states. Furthermore, we will integrate these results into a comprehensive assessment method including the global behavior of masonry structures.

ACKNOWLEDGMENTS

The present investigation was developed in the framework of the Research Program FAR 2020 of the University of Ferrara. Moreover, the analyses were carried out within the activities of the (Italian) University Network of Seismic Engineering Laboratories–ReLUIS in the research program funded by the (Italian) National Civil Protection—Progetto Esecutivo 2019/21—WP2, Unique Project Code (CUP) F54I19000040005. The contributions of Drs. Riccardo Lamborghini and Marco Rigolin to the buildings survey is gratefully acknowledged.

REFERENCES

ABK (1981) Methodology for mitigation of seismic hazards in existing unreinforced masonry building: wall testing, out plane. El Segundo, California

Beer M, Ferson S, Kreinovich V (2013) Imprecise probabilities in engineering analyses. Mech Syst Signal Process 37:4–29. doi: 10.1016/j.ymssp.2013.01.024

Bindi D, Pacor F, Luzi L, et al (2011) Ground motion prediction equations derived from the Italian strong motion database. Bull Earthq Eng 9:1899–1920. doi: 10.1007/s10518-011-9313-z

Boscato G, Pizzolato M, Russo S, Tralli A (2014) Seismic Behavior of a Complex Historical Church in L'Aquila. Int J Archit Herit 8:718–757. doi: 10.1080/15583058.2012.736013

CEN (2004) Eurocode 8: Design of structures for earthquake resistance of structures, Part 1.1: General rules, seismic actions and rules for buildings. Brussels

Chiozzi A, Nale M, Tralli A (2017) Fragility assessment of non-structural components undergoing earthquake induced rocking motion. In: Braga F, Salvatore W, Vignoli A (eds) XVII Convegno ANIDIS-L'ingegneria Sismica in Italia. Pisa University Press, Pisa, pp 449–458

de Felice G, Giannini R (2001) Out-of-plane seismic resistance of masonry walls. J Earthq Eng

5:253–271. doi: 10.1080/13632460109350394

Decanini L, De Sortis A, Goretti A, et al (2004) Performance of Masonry Buildings during the 2002 Molise, Italy, Earthquake. Earthq Spectra 20:191–220. doi: 10.1193/1.1765106

Deierlein GG, Krawinkler H, Cornell CA (2003) A framework for performance-based earthquake engineering. In: Pacific Conference on Earthquake Engineering. pp 140–148

DeJong MJ, Dimitrakopoulos EG (2014) Dynamically equivalent rocking structures. Earthq Eng Struct Dyn 43:1543–1563. doi: 10.1002/eqe.2410

Dimitrakopoulos EG, Paraskeva TS (2015) Dimensionless fragility curves for rocking response to near-fault excitations. Earthq Eng Struct Dyn 44:2015–2033. doi: 10.1002/eqe.2571

Doherty K, Griffith MC, Lam N, Wilson J (2002) Displacement-based seismic analysis for out-of-plane bending of unreinforced masonry walls. Earthq Eng Struct Dyn. doi: 10.1002/eqe.126

Dolce M, Speranza E, Dalla Negra R, et al (2015) Constructive Features and Seismic Vulnerability of Historic Centres Through the Rapid Assessment of Historic Building Stocks. The Experience of Ferrara, Italy. pp 165–175

Giresini L, Fragiacomo M, Lourenço PB (2015) Comparison between rocking analysis and kinematic analysis for the dynamic out-of-plane behavior of masonry walls. Earthq Eng Struct Dyn 44:2359–2376. doi: 10.1002/eqe.2592

Giuffré A (1996) A Mechanical Model for Statics and Dynamics of Historical Masonry Buildings. In: Protection of the Architectural Heritage Against Earthquakes. Springer Vienna, Vienna, pp 71–152

Graziotti F, Tomassetti U, Penna A, Magenes G (2016) Out-of-plane shaking table tests on URM single leaf and cavity walls. Eng Struct 125:455–470. doi: 10.1016/j.engstruct.2016.07.011

Housner GW (1963) The behavior of inverted pendulum structures during earthquakes. Bull Seismol Soc Am 53:403–417

Housner GW (1965) Intensity of Earthquake Ground Shaking Near the Causative Fault. In: 3rd World Conference on Earthquake Engineering. pp 94–115

Indirli M, S. Kouris LA, Formisano A, et al (2013) Seismic Damage Assessment of Unreinforced Masonry Structures After The Abruzzo 2009 Earthquake: The Case Study of the Historical Centers of L'Aquila and Castelvecchio Subequo. Int J Archit Herit 7:536–578. doi: 10.1080/15583058.2011.654050

Krawinkler H, Miranda E (2004) Performance-Based Earthquake Engineering. In: Bozorgnia Y, Bertero V V. (eds) Earthquake Engineering from Engineering Seismology to Performance-Based Engineering. CRC press, p 976

Lagomarsino S (2015) Seismic assessment of rocking masonry structures. Bull Earthq Eng 13:97–128. doi: 10.1007/s10518-014-9609-x

Lagomarsino S, Giovinazzi S (2006) Macroseismic and mechanical models for the vulnerability and damage assessment of current buildings. Bull Earthq Eng 4:415–443. doi: 10.1007/s10518-006-9024-z

Mauro A, de Felice G, DeJong MJ (2015) The relative dynamic resilience of masonry collapse mechanisms. Eng Struct 85:182–194. doi: 10.1016/j.engstruct.2014.11.021

Ministero delle Infrastrutture e dei Trasporti (2018) D.M. 17.01.18 Aggiornamento delle "Norme Tecniche per le costruzioni." Ministero delle Infrastrutture e dei Trasporti, Italy

Ministero delle Infrastrutture e dei Trasporti (2019) CIRCOLARE 21 gennaio 2019 , n. 7 C.S.LL.PP. . Istruzioni per l'applicazione dell'«Aggiornamento delle "Norme tecniche per le costruzioni"»

di cui al decreto ministeriale 17 gennaio 2018.

Nale M, Chiozzi A, Lamborghini R, et al (2020) Fragility assessment of unreinforced masonry walls undergoing earthquake-induced local failure mechanisms. In: Papadrakakis M, Fragiadakis M, Papadimitriou C (eds) EURODYN 2020 Proceedings. European Association for Structural Dynamics, Athens, pp 4311–4317

Penna A, Morandi P, Rota M, et al (2014) Performance of masonry buildings during the Emilia 2012 earthquake. Bull Earthq Eng 12:2255–2273. doi: 10.1007/s10518-013-9496-6

Pitilakis K, Crowley H, Kaynia AM (eds) (2014) SYNER-G: Typology Definition and Fragility Functions for Physical Elements at Seismic Risk. Springer Netherlands, Dordrecht

Rota M, Penna A, Magenes G (2010) A methodology for deriving analytical fragility curves for masonry buildings based on stochastic nonlinear analyses. Eng Struct 32:1312–1323. doi: 10.1016/j.engstruct.2010.01.009

Shawa O Al, de Felice G, Mauro A, Sorrentino L (2012) Out-of-plane seismic behaviour of rocking masonry walls. Earthq Eng Struct Dyn 41:949–968. doi: 10.1002/eqe.1168

Silva V, Akkar S, Baker J, et al (2019) Current Challenges and Future Trends in Analytical Fragility and Vulnerability Modelling. Earthq Spectra. doi: 10.1193/042418EQS101O

Simões AG, Bento R, Lagomarsino S, et al (2020) Seismic assessment of nineteenth and twentieth centuries URM buildings in Lisbon: structural features and derivation of fragility curves. Bull Earthq Eng 18:645–672. doi: 10.1007/s10518-019-00618-z

Simões AG, Bento R, Lagomarsino S, et al (2019a) Fragility Functions for Tall URM Buildings around Early 20th Century in Lisbon. Part 1: Methodology and Application at Building Level. Int J Archit Herit 1–24. doi: 10.1080/15583058.2019.1618974

Simões AG, Bento R, Lagomarsino S, et al (2019b) Fragility Functions for Tall URM Buildings around Early 20th Century in Lisbon, Part 2: Application to Different Classes of Buildings. Int J Archit Herit 1–17. doi: 10.1080/15583058.2019.1661136

Sorrentino L, AlShawa O, Decanini LD (2011) The relevance of energy damping in unreinforced masonry rocking mechanisms. Experimental and analytic investigations. Bull Earthq Eng 9:1617–1642. doi: 10.1007/s10518-011-9291-1

Sorrentino L, Cattari S, da Porto F, et al (2019) Seismic behaviour of ordinary masonry buildings during the 2016 central Italy earthquakes. Bull Earthq Eng 17:5583–5607. doi: 10.1007/s10518-018-0370-4

Sorrentino L, D'Ayala D, de Felice G, et al (2016) Review of Out-of-Plane Seismic Assessment Techniques Applied To Existing Masonry Buildings. Int J Archit Herit 1–20. doi: 10.1080/15583058.2016.1237586

Sorrentino L, Masiani R, Griffith MC (2008) The vertical spanning strip wall as a coupled rocking rigid body assembly. Struct Eng Mech 29:433–453. doi: 10.12989/sem.2008.29.4.433

Spanos PD, Koh A (1984) Rocking of Rigid Blocks Due to Harmonic Shaking. J Eng Mech 110:1627–1642. doi: 10.1061/(ASCE)0733-9399(1984)110:11(1627)

Spillatura A, Fiorini E, Bazzurro P, Pennucci D (2014) Harmonization of vulnerability fragility curves for masonry buildings. In: Second European Conference on Earthquake Engineering

Suzuki A, Iervolino I (2017) Italian vs. worldwide history of largest PGA and PGV. Ann Geophys 60:. doi: 10.4401/ag-7391

The Mathworks Inc. (2016) MATLAB - MathWorks. In: www.mathworks.com/products/matlab. http://www.mathworks.com/products/matlab/

Tomassetti U, Graziotti F, Sorrentino L, Penna A (2019) Modelling rocking response via equivalent viscous damping. Earthq Eng Struct Dyn 48:1277–1296. doi: 10.1002/eqe.3182

Whittaker A, Atkinson G, Baker J, et al (2011) Selecting and Scaling Earthquake Ground Motions for Performing Response-History Analyses

Yim C-S, Chopra AK, Penzien J (1980) Rocking response of rigid blocks to earthquakes. Earthq Eng Struct Dyn 8:565–587. doi: 10.1002/eqe.4290080606

Zio E (2013) The Monte Carlo Simulation Method for System Reliability and Risk Analysis. Springer London, London

Zuccaro G, Dato F, Cacace F, et al (2017) Seismic collapse mechanisms analyses and masonry structures typologies: a possible correlation. Ing Sismica 34:121–149

Zuccaro G, Dolce M, De Gregorio D, et al (2016) La Scheda Cartis Per La Caratterizzazione Tipologico- Strutturale Dei Comparti Urbani Costituiti Da Edifici Ordinari. Valutazione dell'esposizione in analisi di rischio sismico. Gngts 2015

FIGURES

Figure 17: comparison between the average curves obtained from the population created from the Cartis database and the average curves obtained from the survey of the historical aggregate: difference between the typological survey curve (back line), the typological curve MUR1 (blue line) and the typological curve MUR2 (red line)

Figure 1: the historical aggregate in the center of Ferrara, Italy (aerial view).

a) b)

Figure 2: example of buildings MUR1 class

a) b)

Figure 3: example of buildings MUR 2 class

a) b) c) d)

Figure 4: types of clay brick wall in Ferrara for MUR1 and MUR2 class

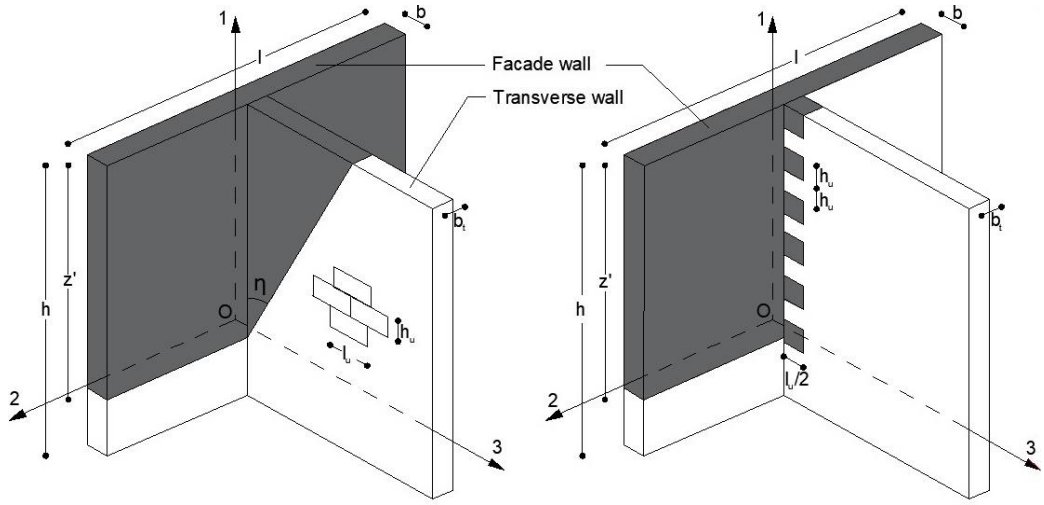

Figure 5: Out-of-plane collapse mechanisms taking into account connections with transversal walls (de Felice and Giannini 2001).

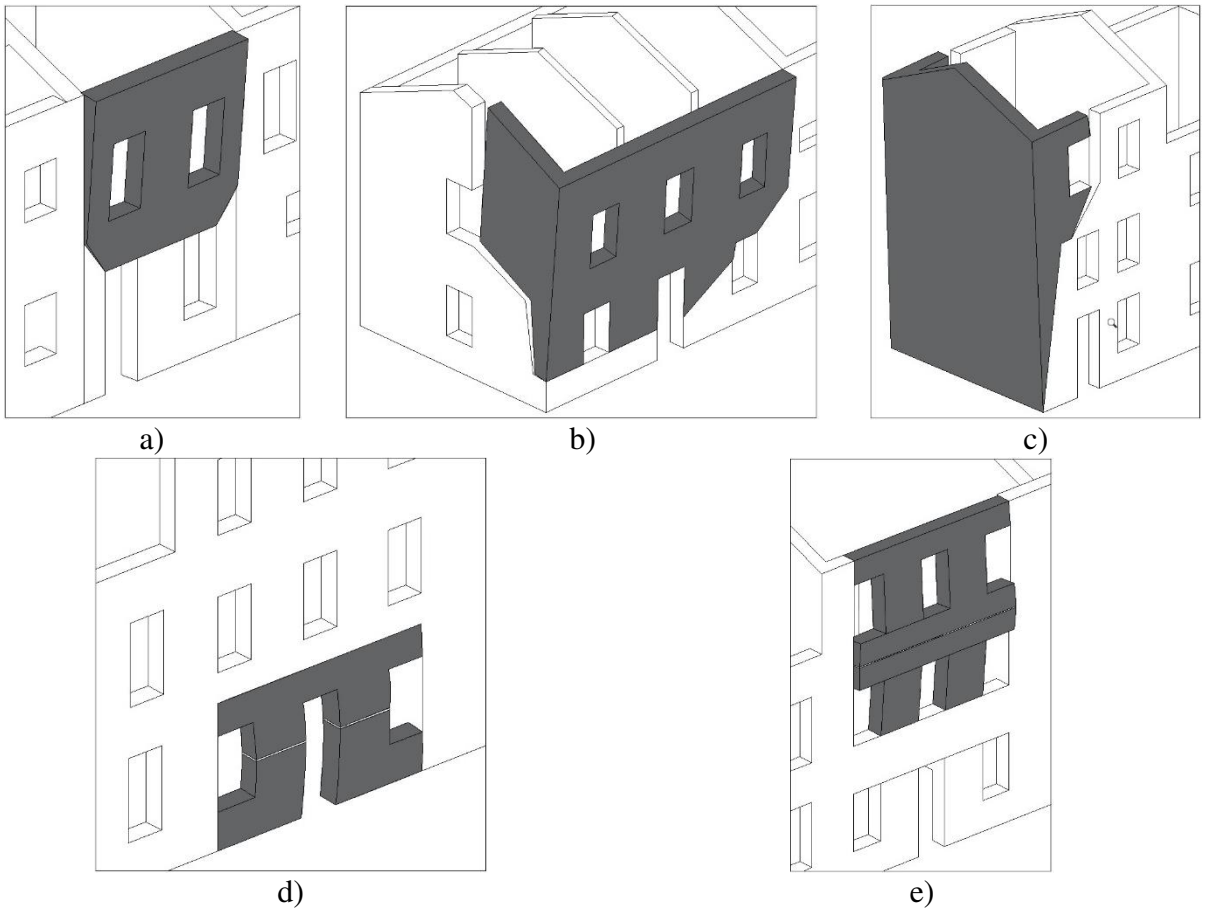

Figure 6: example of out-of-plane wall overturning in unreinforced masonry buildings a) overturning of a wall at first-floor b) partial overturning of the facade, c) total overturning of the facade, d) flexural mechanism of a wall, e) flexural mechanism of the facade

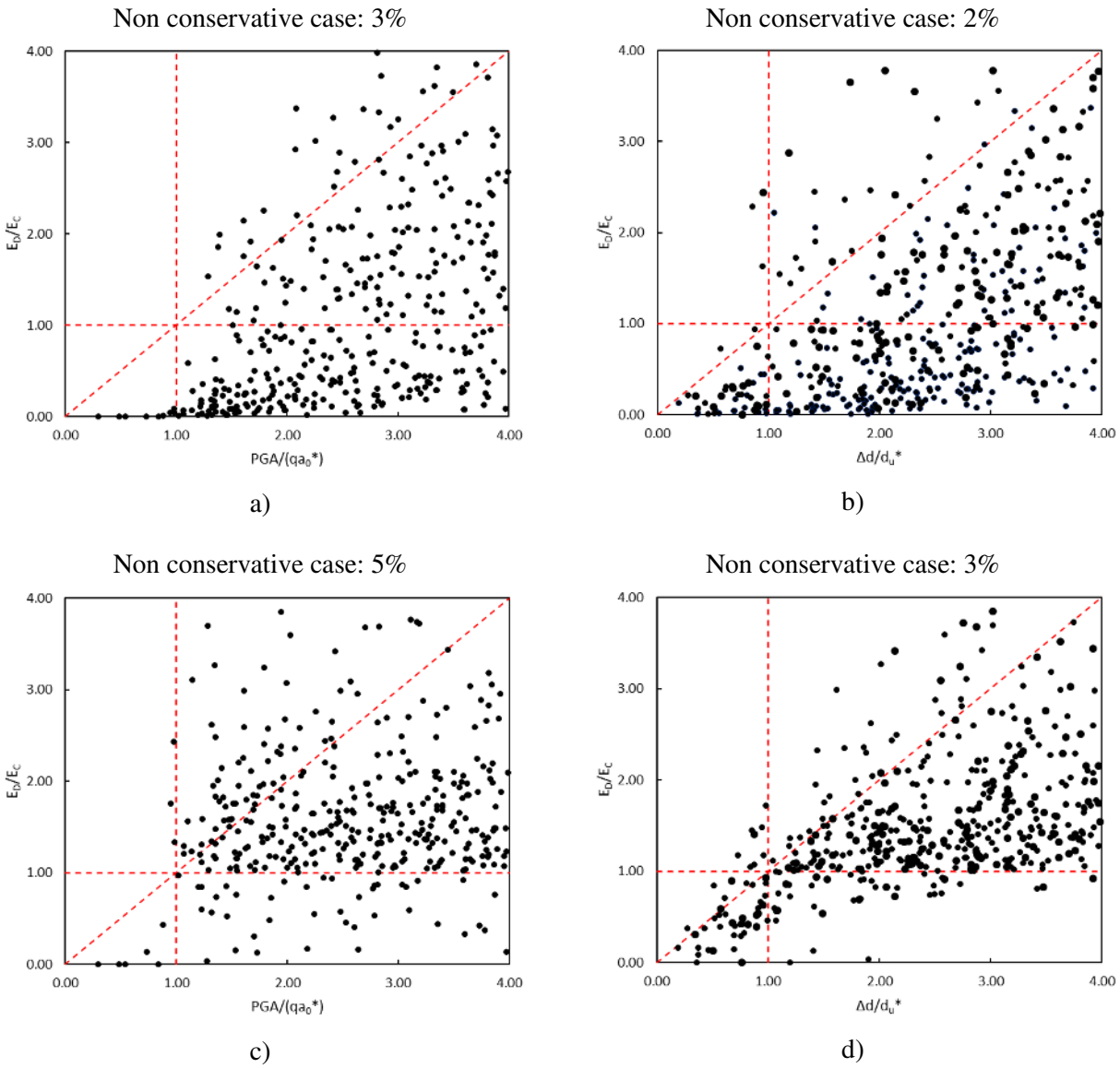

Figure 7: Comparison between Italian code (NTC 2018) and non-linear dynamic analysis: a) static force-based approach for one-sided rocking, b) displacement-based approach for one-sided rocking, c) static force-based approach for vertical bending, b) displacement-based approach for vertical bending.

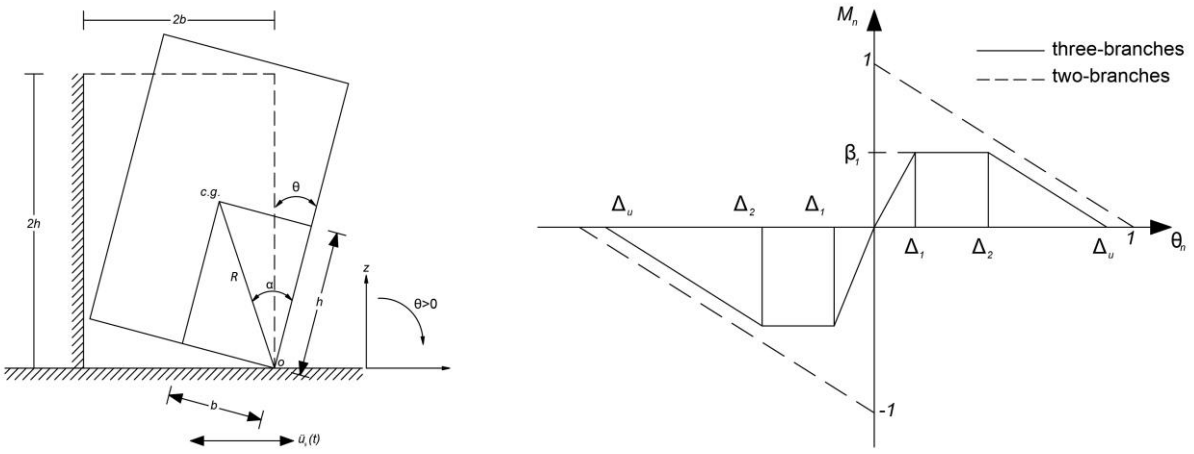

Figure 8: a) geometry of a rigid block under the one-sided rocking under ground motion, b) normalized moment-rotation relationship.

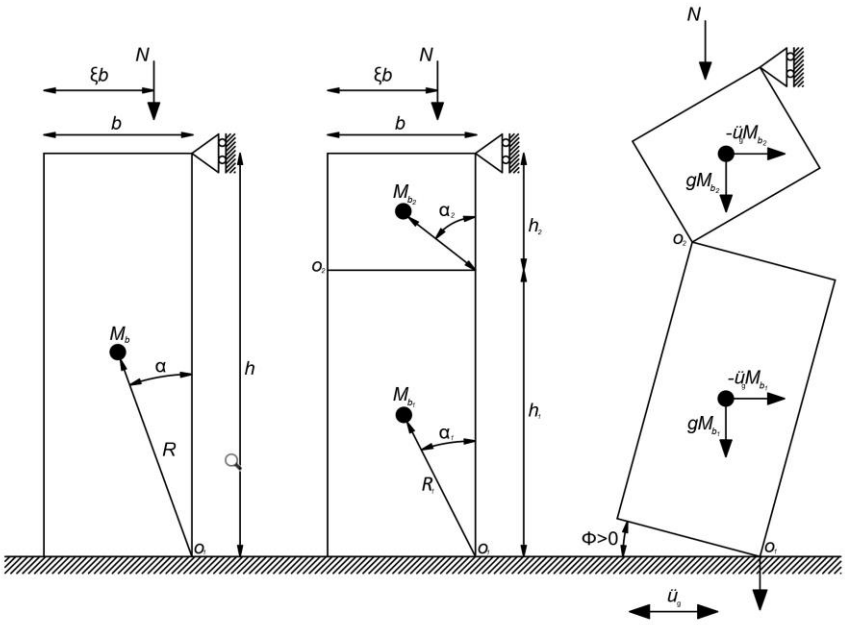

Figure 9: (a) wall parameters, (b) cracked vertical spanning strip wall parameters, (c) displaced configuration and ground acceleration component acting in the mass centers of the two bodies

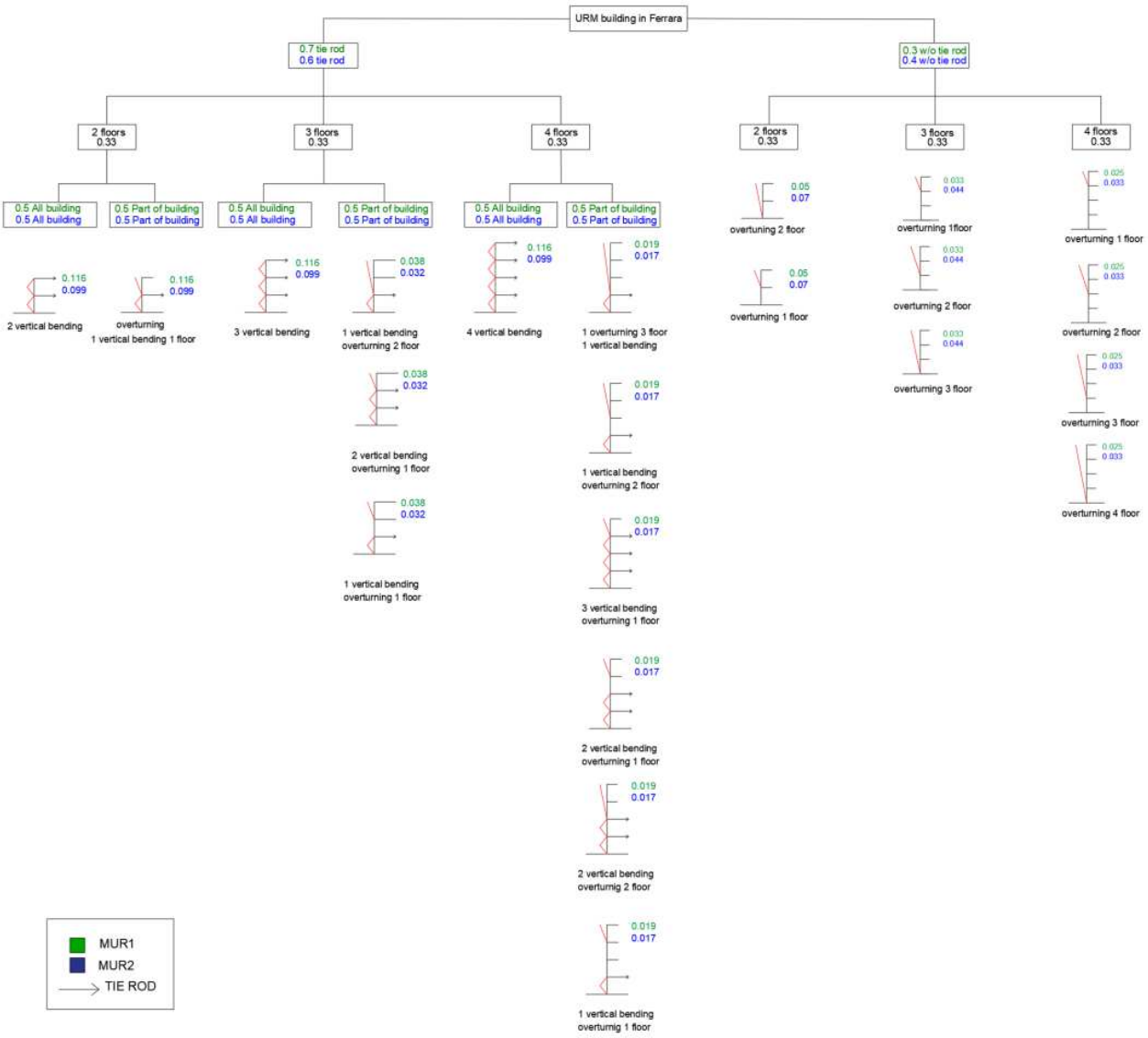

Figure 10: logic-tree for URM buildings in Ferrara of the possible local mechanisms with relative weights (green for the MUR 1 typology and blue for MUR2 typology)

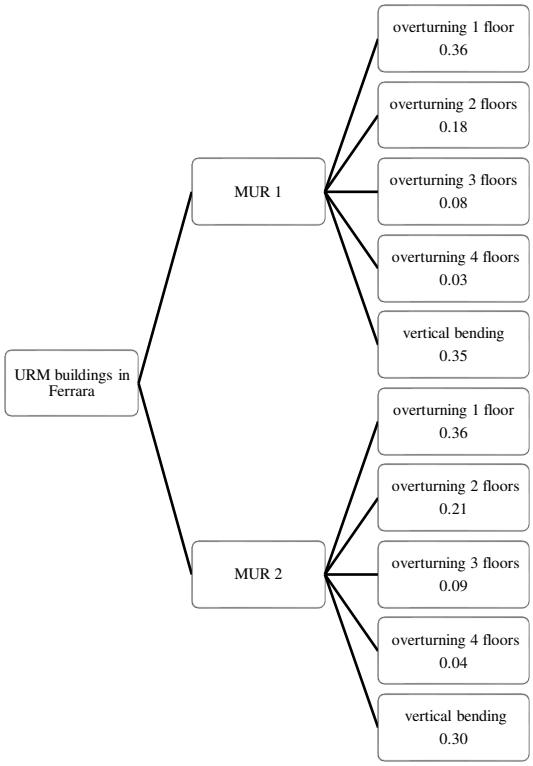

Figure 11: diagram of the relative weights for each type of collapse mechanism

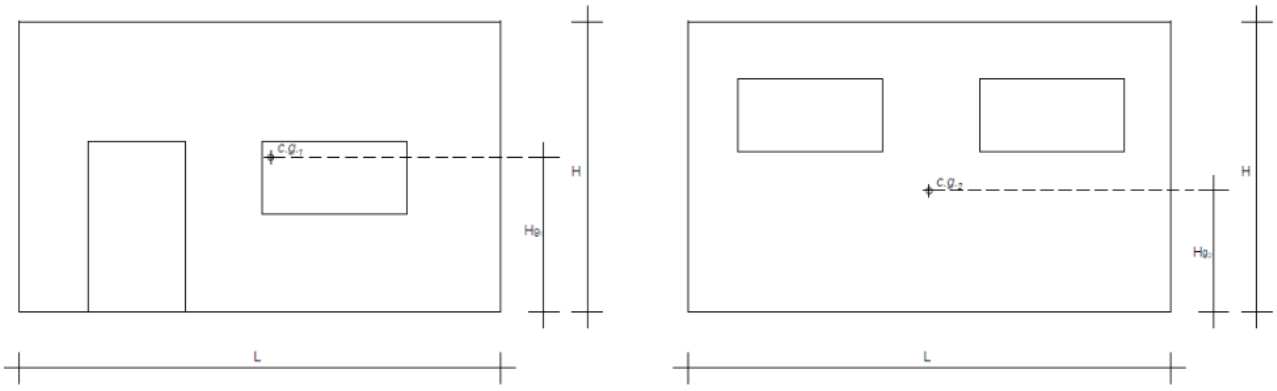

Figure 12: different possible combinations of wall with different types of openings

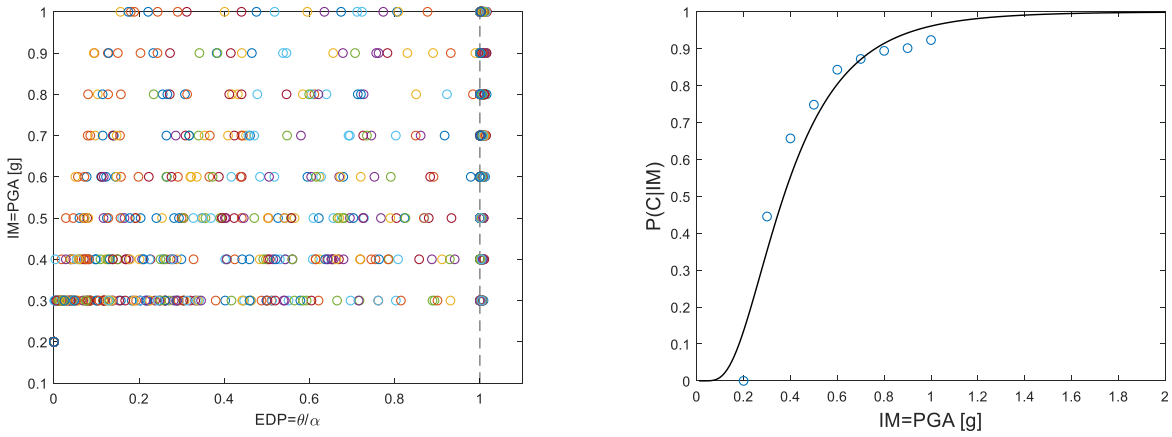

a) b)

Figure 13: example MSA analysis results; a) analyses causing collapse are plotted at a critical angle of greater than 1.0 and are offset from each other to aid in visualizing the number of collapses. b) Observed fractions of collapse as a function of IM, and a fragility function estimated using equation 16

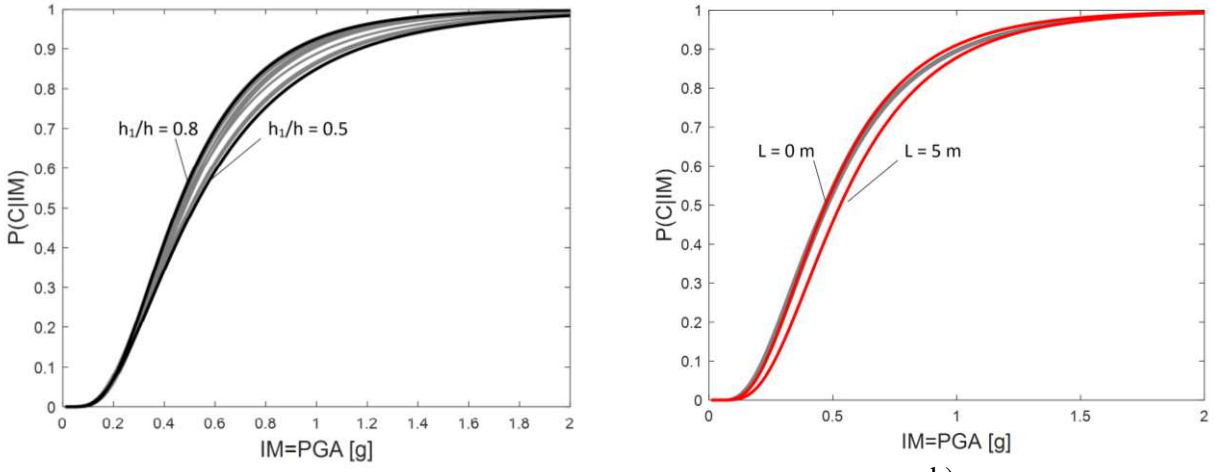

a) b)

Figure 14: sensitivity of the fragility parameters for vertical bending mechanism: a) variation of the position of hinge (h_l/h from 0.5 to 0.8), b) variation of the vertical force N; as effect of the span of the slab (L from 0 m to 5 m) on vertical force (red lines)

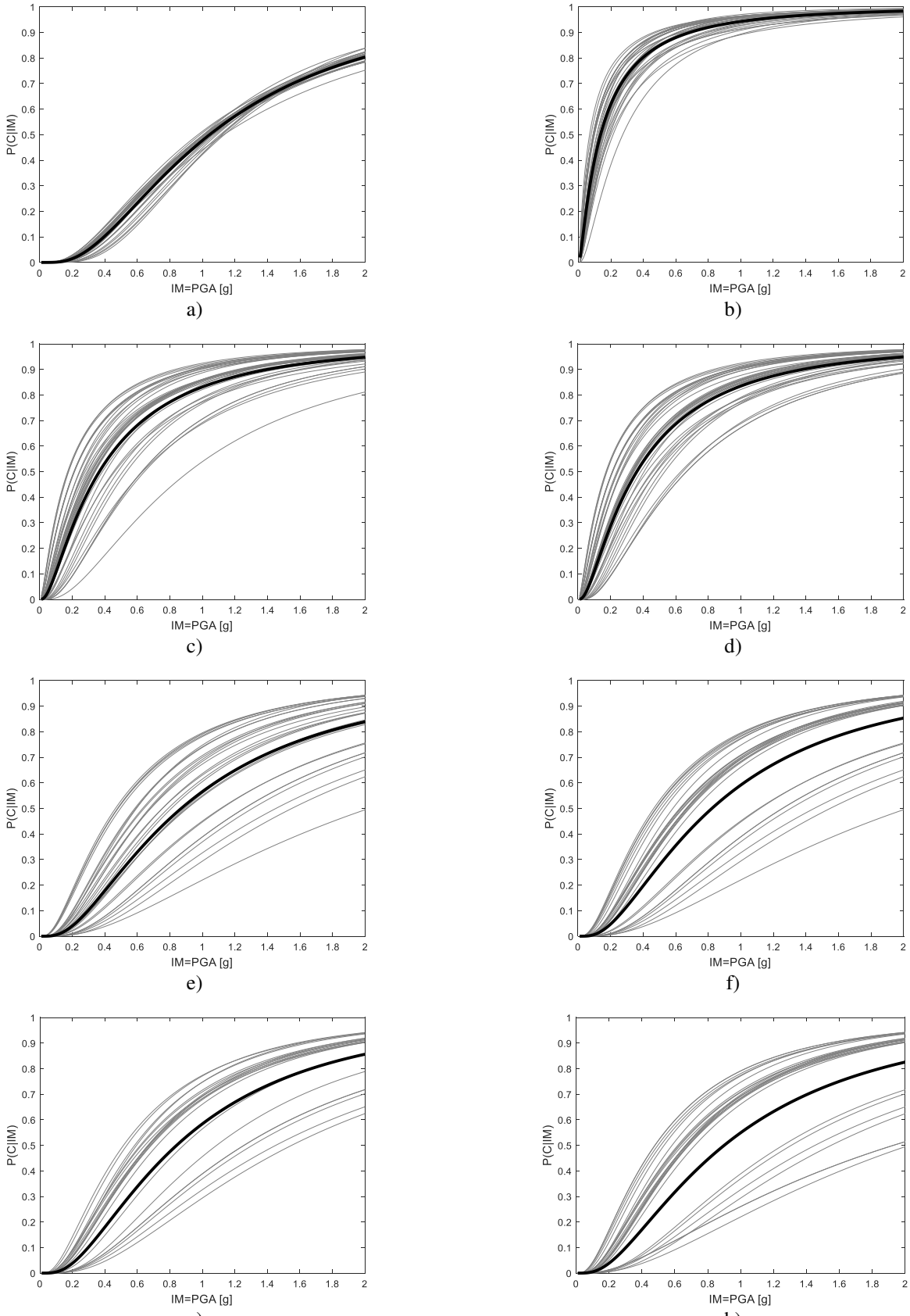

Figure 15: fragility curves from CARTIS database: a) top floor vertical bending, b) overturning of the first floor, c) overturning of two floors for MUR1, d) overturning of two floors for MUR2 class, e) overturning of three floors for MUR1 class f) overturning of three floors for MUR2 class, g) overturning of four floors for MUR1 class, h) overturning of four floors for MUR2 class

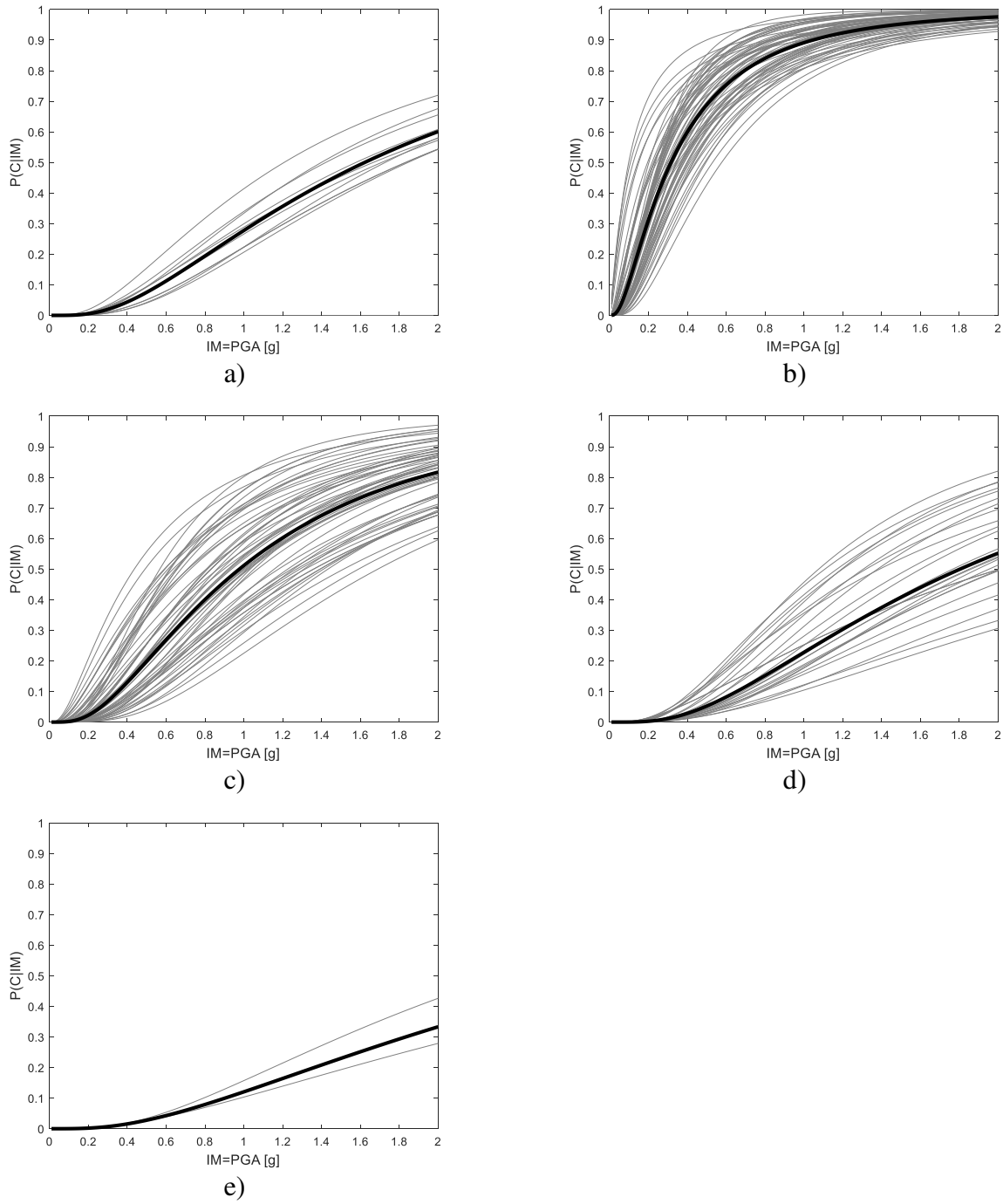

Figure 16: fragility curves from the survey of the historical aggregate in the center of Ferrara: a) vertical bending, b) overturning of the first floor, c) overturning of two floors, e) overturning of three floors

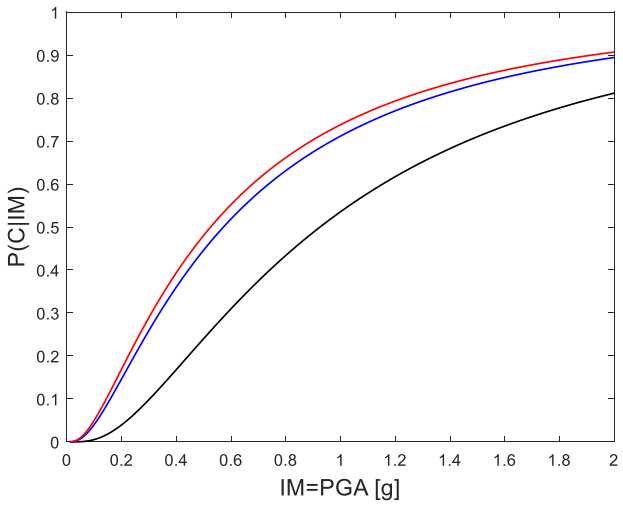

Figure 17: comparison between the average curves obtained from the population created from the Cartis database and the average curves obtained from the survey of the historical aggregate: difference between the typological survey curve (back line), the typological curve MUR1 (blue line) and the typological curve MUR2 (red line)

TABLES

Table 1: parameters of buildings

Table 2: block used in the analysis, b is the thickness of the wall whereas h is the height of the wall

Table 3: the trilateral moment rotation curves parameters

Table 4: Italian ground motion records with important recorded PGA and PGV (†EC8 classification (CEN 2004), *Epicentral distance, [I] = ITACA, [E]=ESM).

Table 5: performance criteria for rocking behavior

Table 1: parameters of buildings

Parameters	MUR 1	MUR 2
Number of floors	2 - 4	2 - 4
Average floor height [m]	2.5 – 3-5	2.5 – 3.5
Average ground floor height [m]	3.5 – 5.0	2.5 – 3.5
Average floor area [m^2]	100 – 230	70 – 170
Age of building	before 1860 1861 – 1919	1919 - 1945
Type of masonry	Clay brick wall	Clay brick wall
Transversal connections	No information	No information
With tie rods or tie beams	70%	60%
Average thickness of ground floor walls [cm]	30	30
Average distance between walls parallel to the facade [m]	5.5	4.5
type of slab	wood	wood
type of roof	Wooden - not pushing	Wooden - not pushing

Table 2: block used in the analysis, b is the thickness of the wall whereas h is the height of the wall

Wall	b [m]	h [m]	boundary conditions
1	0.25	4	one-sided rocking two-block mechanism
2	0.25	7.5	one-sided rocking two-block mechanism
3	0.25	11.2	one-sided rocking two-block mechanism

Table 3: the trilateral moment rotation curves parameters

State of degradation	Δ_1/Δ_u	Δ_2/Δ_u
New	6 %	28 %
Moderate	13 %	40 %
Severe	20 %	50 %

Table 4: Italian ground motion records with important recorded PGA and PGV (†EC8 classification (CEN 2004), *Epicentral distance, [I] = ITACA, [E]=ESM).

Year	Event	Event id	Station (Station code, Soil class†)	Focal mechanism	Magnitude M_w (M_L)	Distance* [km]	PGA [g]	PGV [cm/s]	Source
1972	Ancona	IT-1972-0005	Ancona, Rocca (ANR,B)	Unknown	(4,7)	7.7	0.55	9,9	[I]
1976	Friuli 1st shock	IT-1976-0002	Tolmezzo Centrale (TLM1,B)	Thrust	6.4	27.7	0.35	30,2	[I]
1976	Friuli aftershock	IT-1976-0027	Gemona (GMN, B)	Thrust	5.9	6.2	0.63	68,4	[I]
1976	Friuli 3rd shock	IT-1976-0030	Folgaria Cornino (FRC, B)	Thrust	6.0	16.2	0.34	23,7	[I]
1976	Friuli 3rd shock	IT-1976-0030	Gemona (GMN, B)	Thrust	6.0	4.0	0.25	30,5	[I]
1979	Norcia	IT-1979-0009	Cascia (CSC, B)	Normal	5.8	9.3	0.21	14,5	[I]
1980	Irpinia	IT-1980-0012	Sturno (STR, B)	Normal	6.9	33.3	0.32	70,4	[I]
1984	Lazio-Abruzzo	IT-1984-0004	Cassino-Sant'Elia (SCN0, C)	Normal	5.9	19.7	0.14	11,2	[I]
1990	Potenza	IT-1990-0001	Brienza (BRN, B)	Strike-slip	5.8	29	0.10	6,8	[I]
1997	Umbria Marche 2nd shock	IT-1997-0006	Nocera (NCR. E)	Normal	6.0	10.1	0.49	32,6	[I]
2002	Molise 1st shock	IT-2002-0045	S. Severo (SSV, B)	Strike-slip	5.7	38.1	0.57	2,1	[I]
2009	L'Aquila	IT-2009-0009	L'Aquila - Valterno - Centro Valle (AQV, B)	Normal	6.1	4.9	0.64	42,7	[I]
2009	L'Aquila	IT-2009-0010	L'Aquila - Valterno - Colle Grilli (AQG, B)	Normal	6.1	5	0.48	35,8	[I]
2009	L'Aquila	IT-2009-0011	L'Aquila - Valterno - F. Aterno (AQA, B)	Normal	6.1	5	0.43	31,9	[I]
2009	L'Aquila	IT-2009-0012	L'Aquila - Valterno - Aquil Park Ing. (AQK, B)	Normal	6.1	1.8	0.35	35,8	[I]
2009	L'Aquila aftershock	IT-2009-0102	S. Eusanio Forconese (MI05, B)	Normal	5.5	3.6	0.65	23,6	[I]
2012	Emilia 1st shock	IT-2012-0008	Mirandola (MRN, C)	Thrust	6.1	16.1	0.26	46,3	[I]
2012	Emilia 2nd shock	IT-2012-0011	Carpi (T0814, C)	Thrust	6.0	9.3	0.49	23,6	[I]
2012	Emilia 2nd shock	IT-2012-0011	Medolla (MIR01, C)	Thrust	6.0	0.5	0.41	52,4	[I]
2016	Central Italy	EMSC-20160824_0000006	Amatrice (AMT, B)	Normal	6.0	8.5	0.85	43,5	[ESM]
2016	Central Italy	EMSC-20160824_0000006	Nocera (NRC, B)	Normal	6.0	15.3	0.36	29,8	[ESM]
2016	Central Italy	EMSC-20161030_0000029	Rocchetta (MZ24, C)	Normal	6.5	24.5	1.00	14,3	[ESM]

Table 5: performance criteria for rocking behavior

EDP	Damage state	Structural behavior	Mechanism
$\lvert\phi_{\max}\rvert / \alpha = 1.0$	Collapse	Overturning	One-sided rocking
$\lvert\phi_{\max}\rvert / \alpha_1 = 1.0$	Collapse	Overturning	Two-block mechanism

Figures

Figure 1

the historical aggregate in the center of Ferrara, Italy (aerial view).

Figure 2

example of buildings MUR1 class

Figure 3

example of buildings MUR 2 class

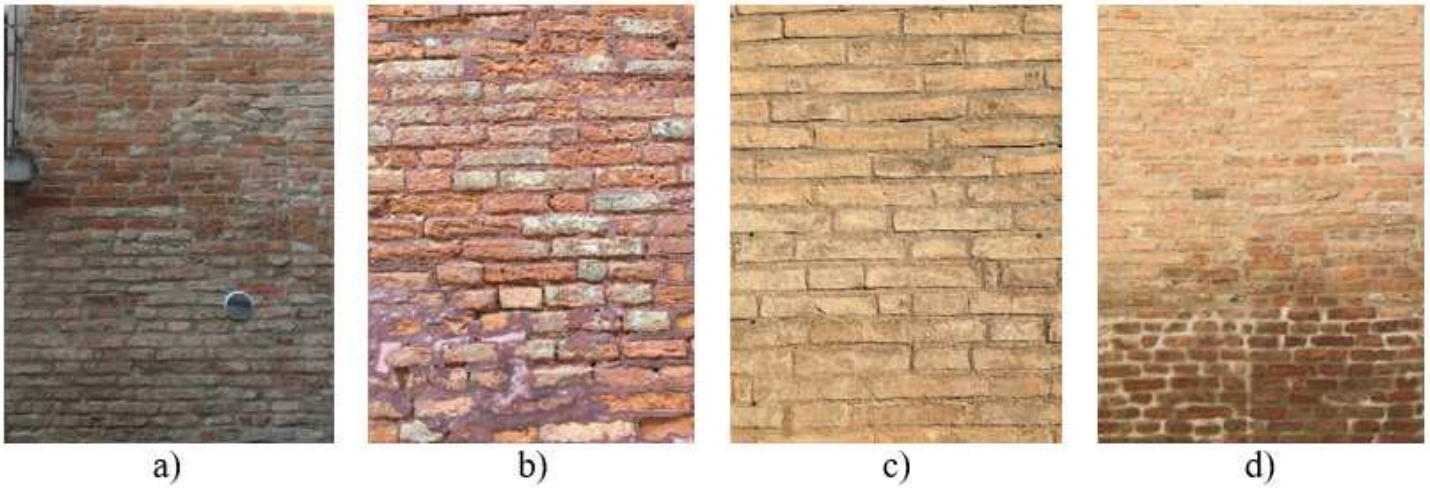

Figure 4

types of clay brick wall in Ferrara for MUR1 and MUR2 class

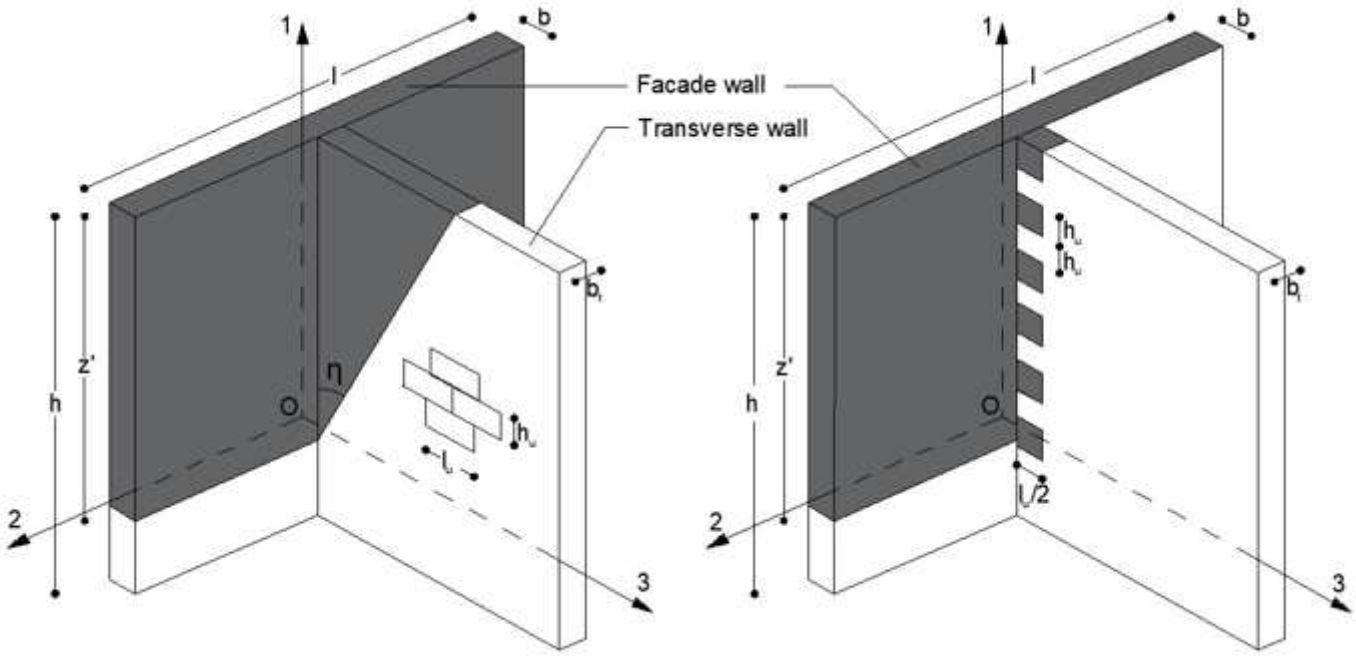

Figure 5

Out-of-plane collapse mechanisms taking into account connections with transversal walls (de Felice and Giannini 2001)

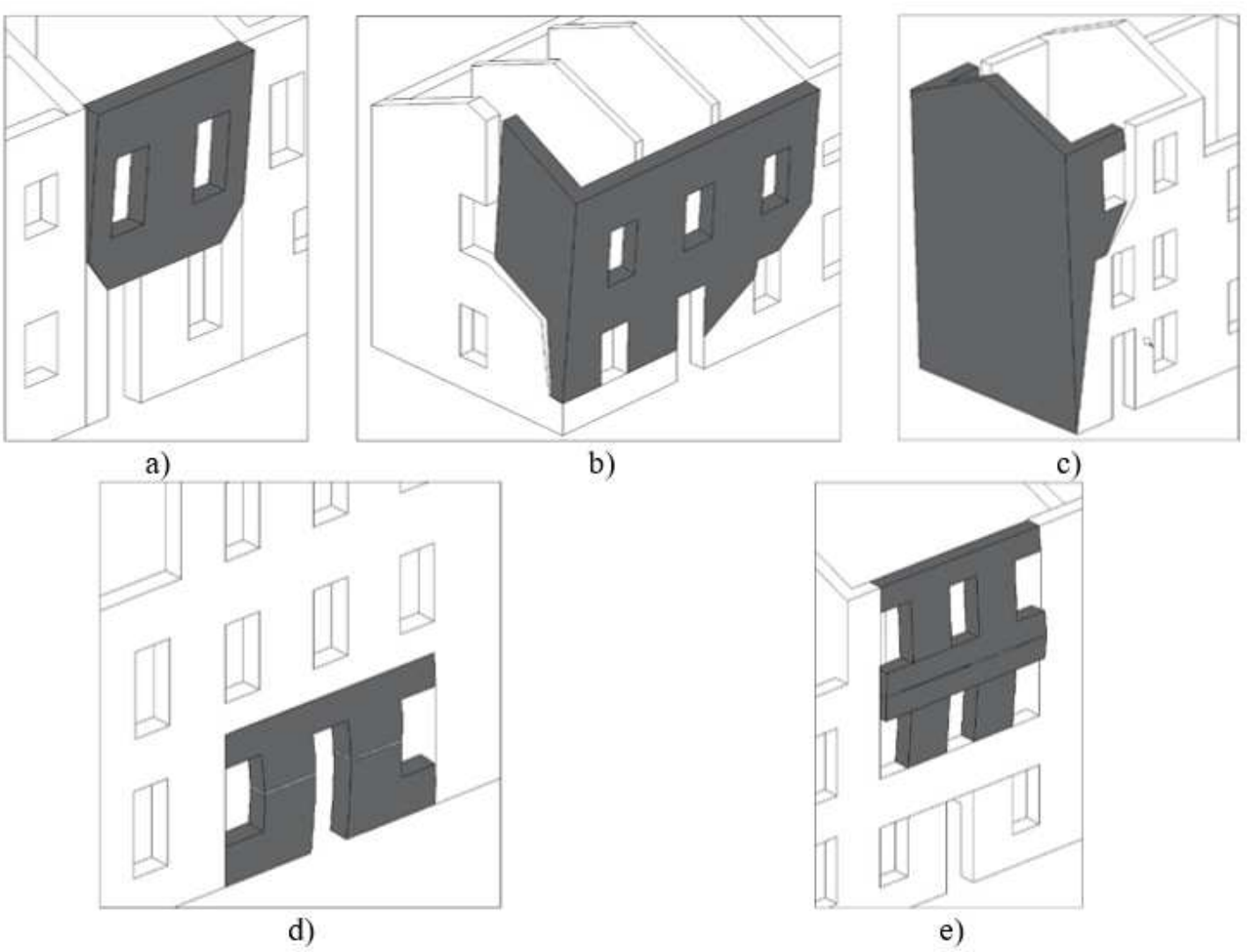

Figure 6

example of out-of-plane wall overturning in unreinforced masonry buildings a) overturning of a wall at first-floor b) partial overturning of the facade, c) total overturning of the facade, d) flexural mechanism of a wall, e) flexural mechanism of the facade

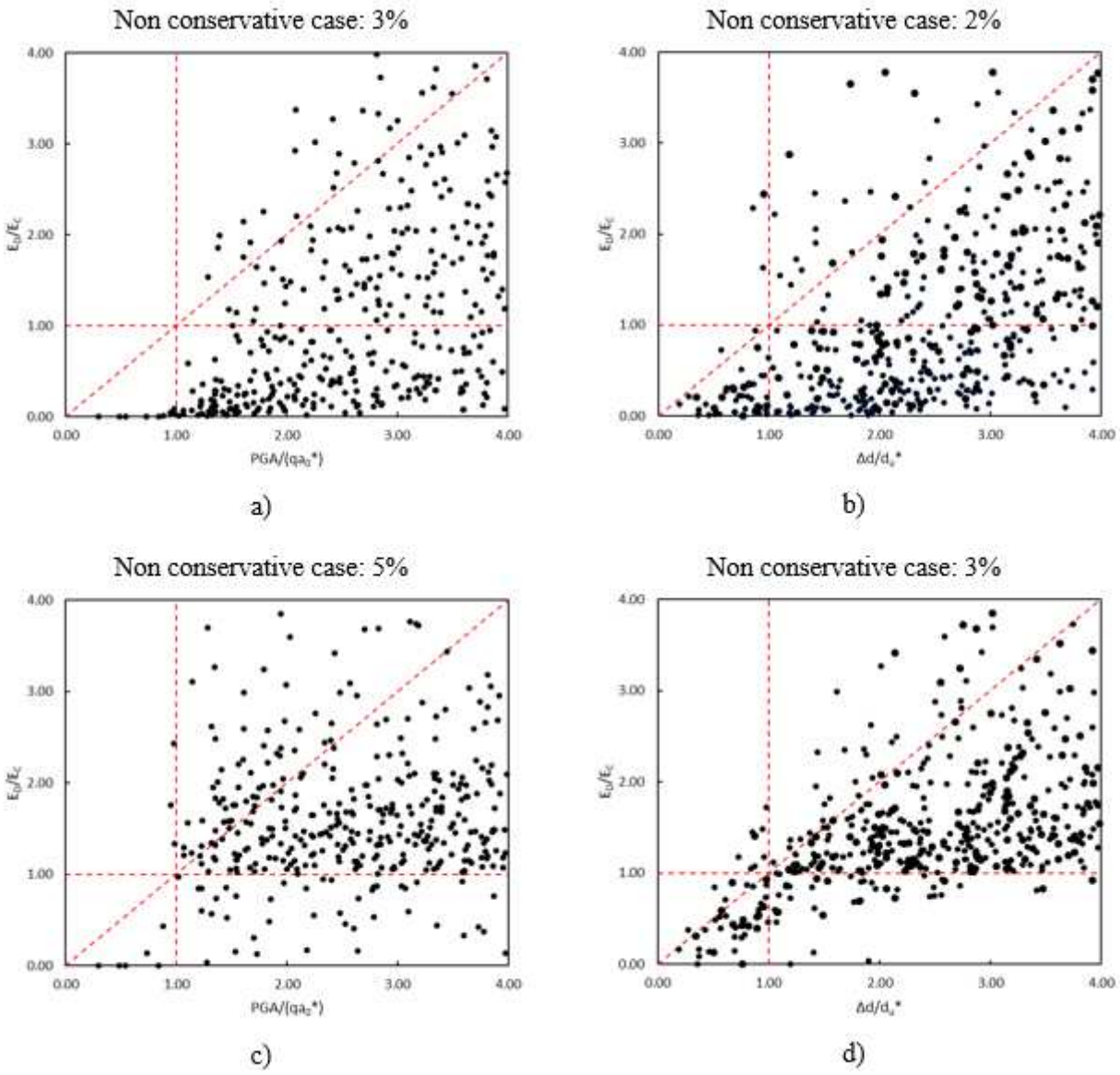

Figure 7

Comparison between Italian code (NTC 2018) and non-linear dynamic analysis: a) static force-based approach for one-sided rocking, b) displacement-based approach for one-sided rocking, c) static force-based approach for vertical bending, b) displacement-based approach for vertical bending.

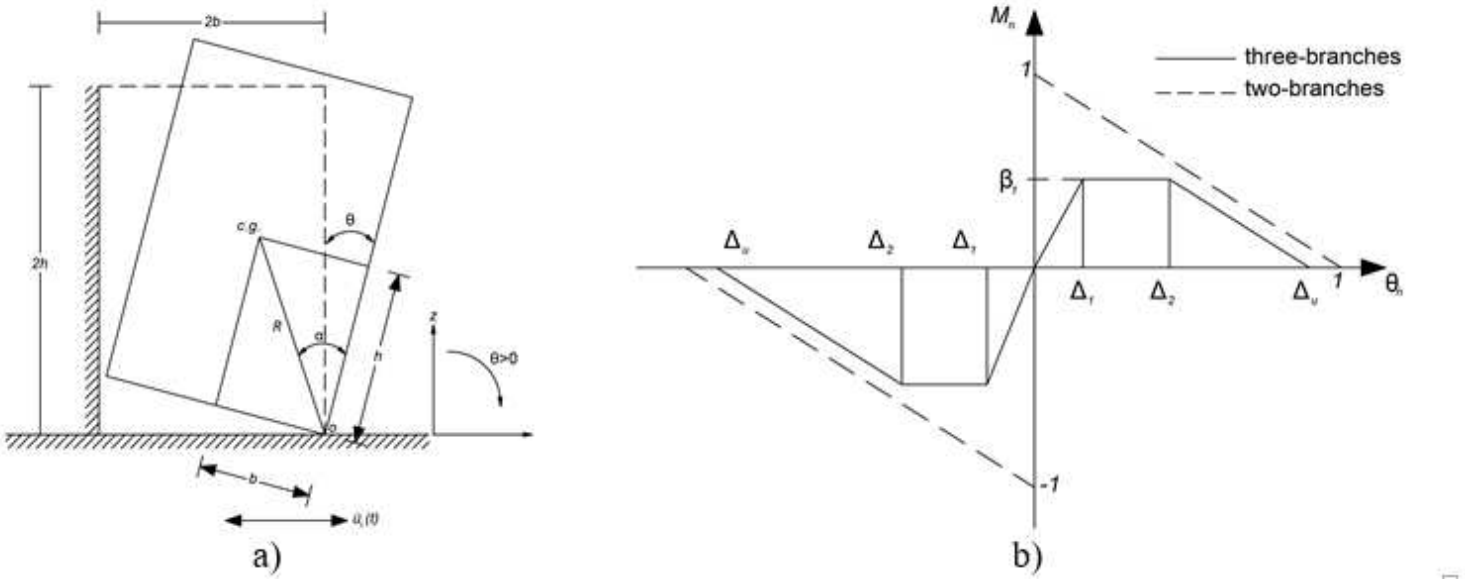

Figure 8

a) geometry of a rigid block under the one-sided rocking under ground motion, b) normalized moment-rotation relationship.

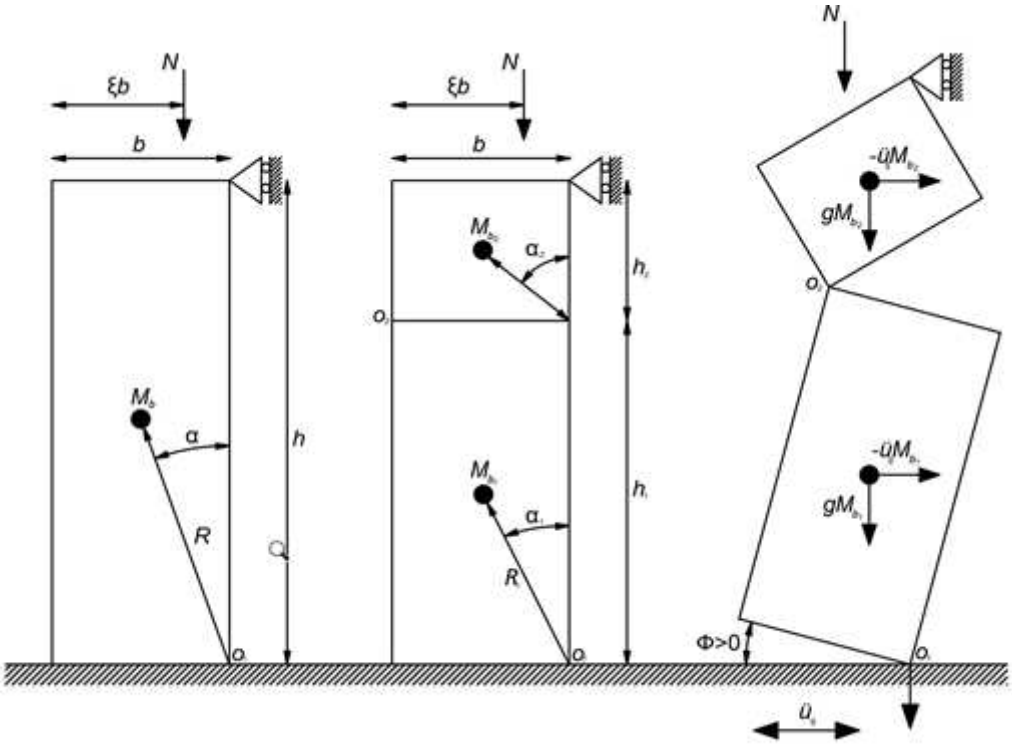

Figure 9

(a) wall parameters, (b) cracked vertical spanning strip wall parameters, (c) displaced configuration and ground acceleration component acting in the mass centers of the two bodies

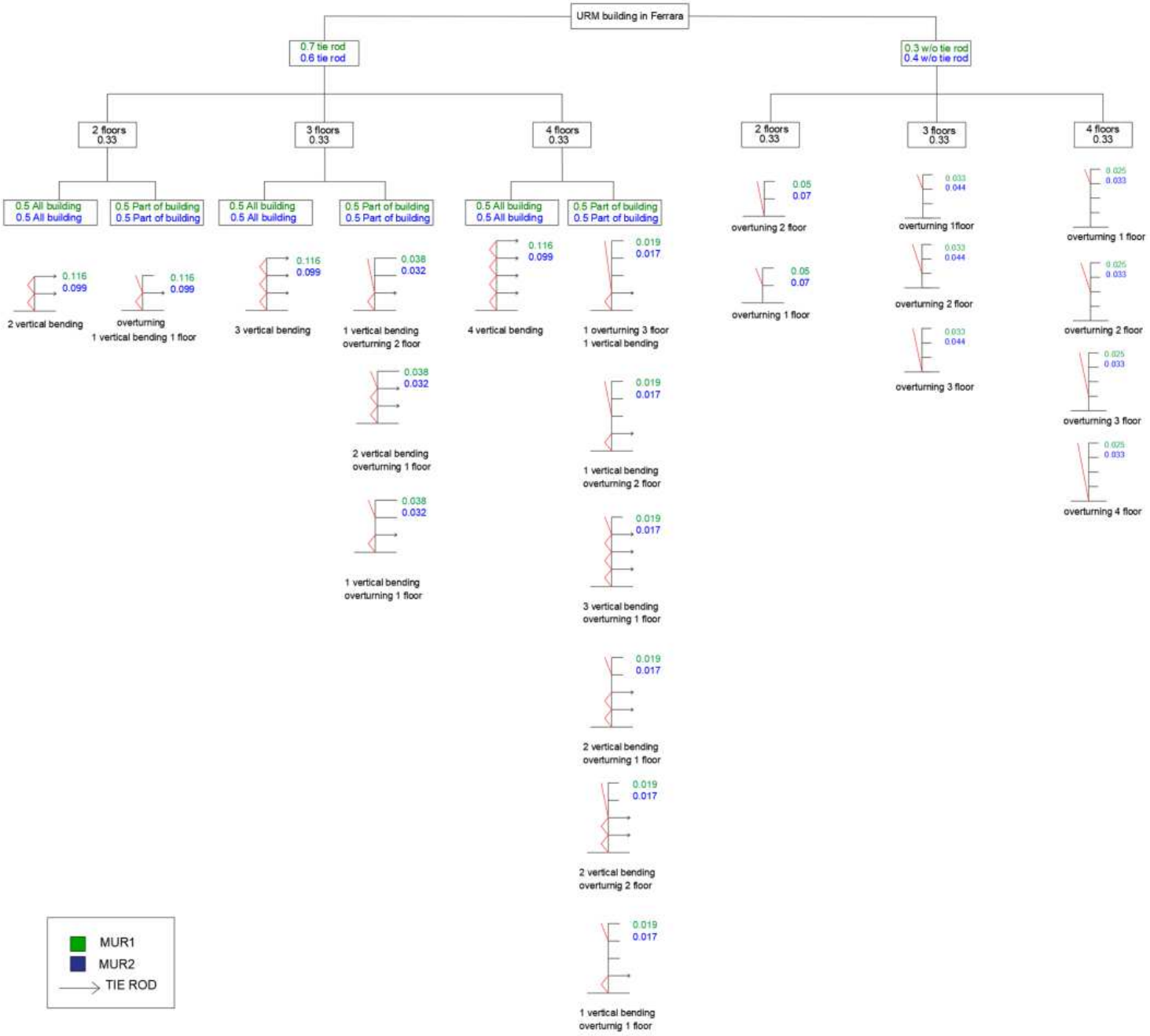

Figure 10

logic-tree for URM buildings in Ferrara of the possible local mechanisms with relative weights (green for the MUR 1 typology and blue for MUR2 typology)

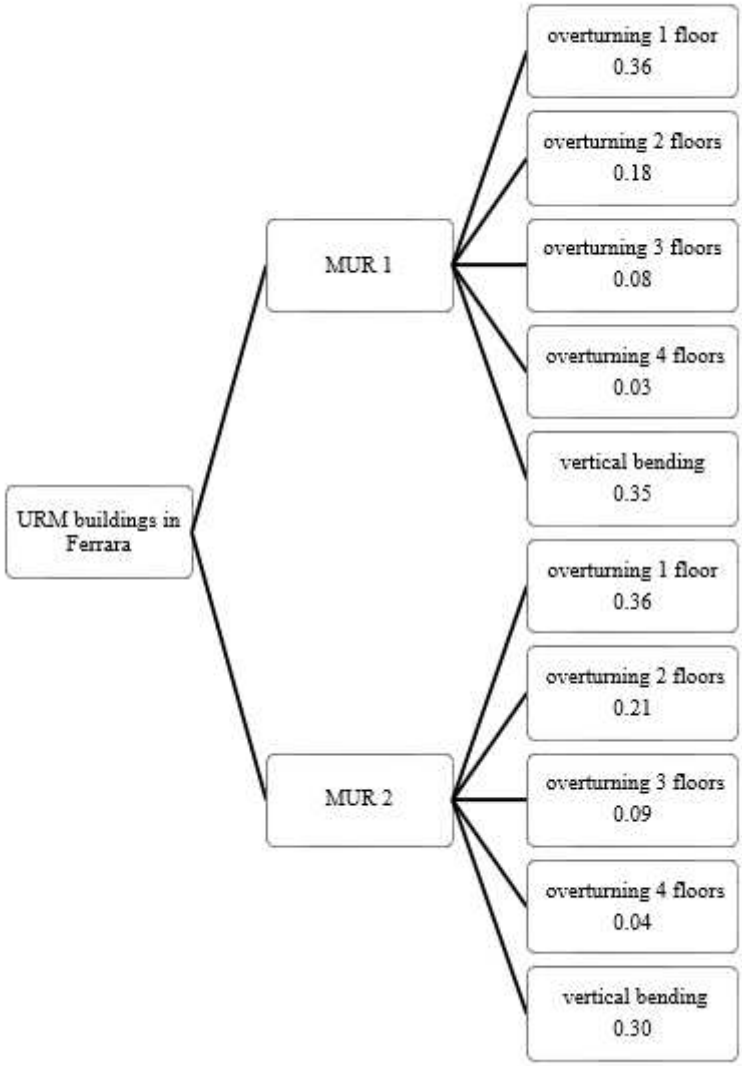

Figure 11

diagram of the relative weights for each type of collapse mechanism

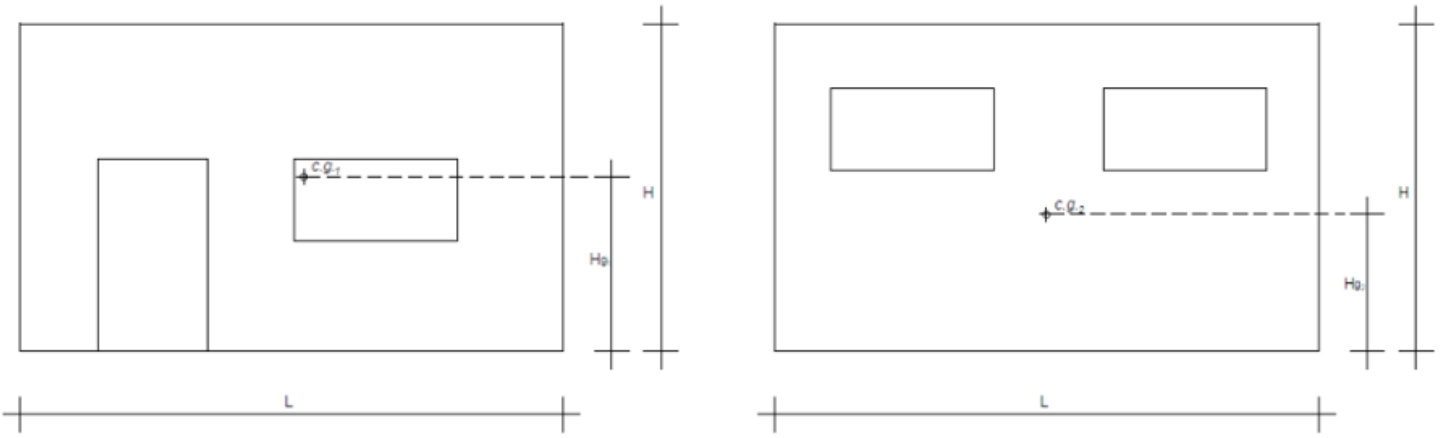

Figure 12

different possible combinations of wall with different types of openings

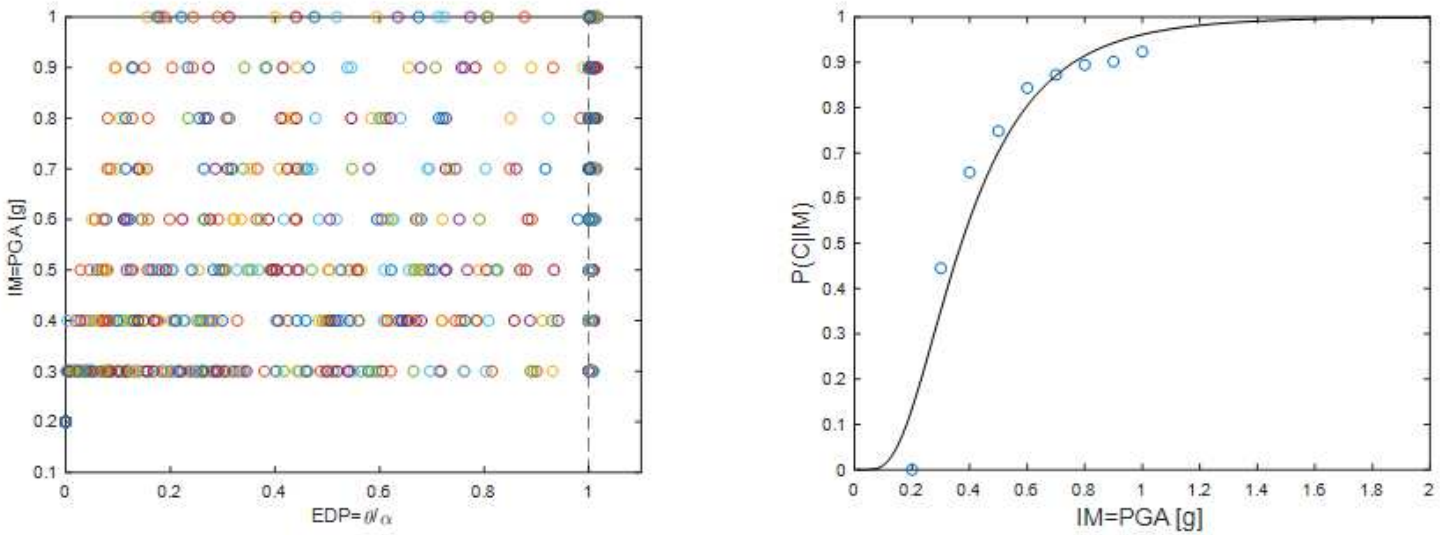

Figure 13

example MSA analysis results; a) analyses causing collapse are plotted at a critical angle of greater than 1.0 and are offset from each other to aid in visualizing the number of collapses. b) Observed fractions of collapse as a function of IM, and a fragility function estimated using equation 16

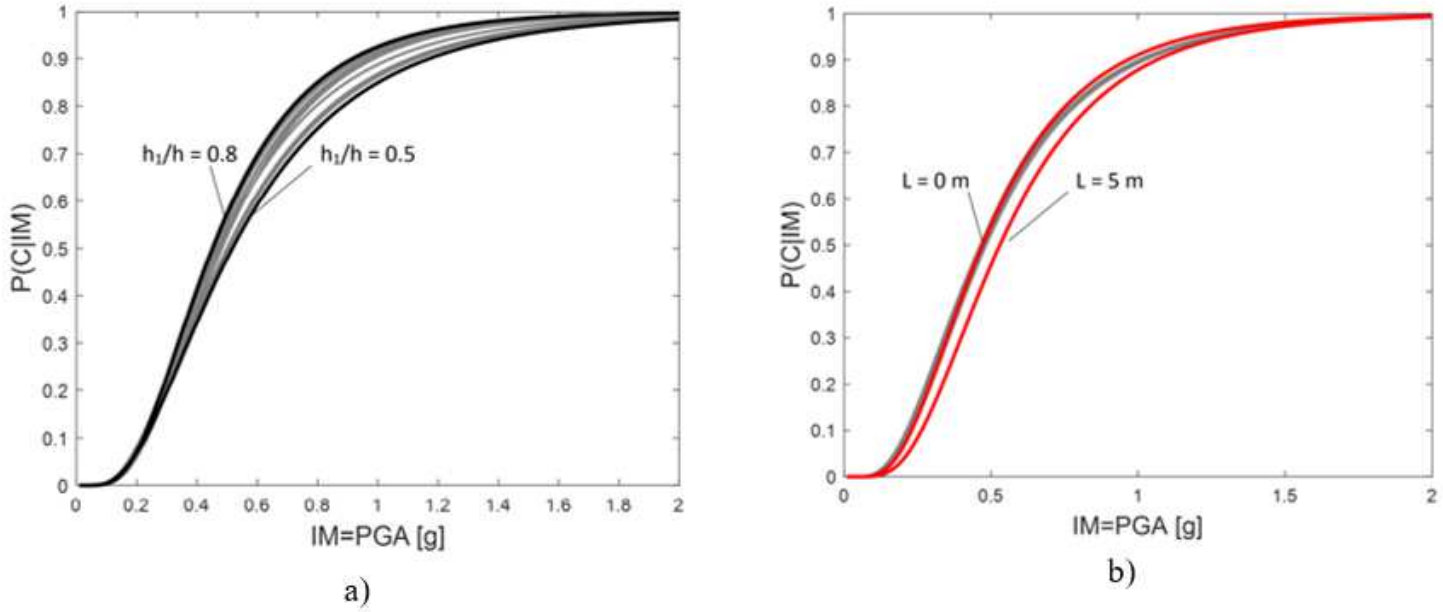

Figure 14

sensitivity of the fragility parameters for vertical bending mechanism: a) variation of the position of hinge (h1/h from 0.5 to 0.8), b) variation of the vertical force N; as effect of the span of the slab (L from 0 m to

5 m) on vertical force (red lines)

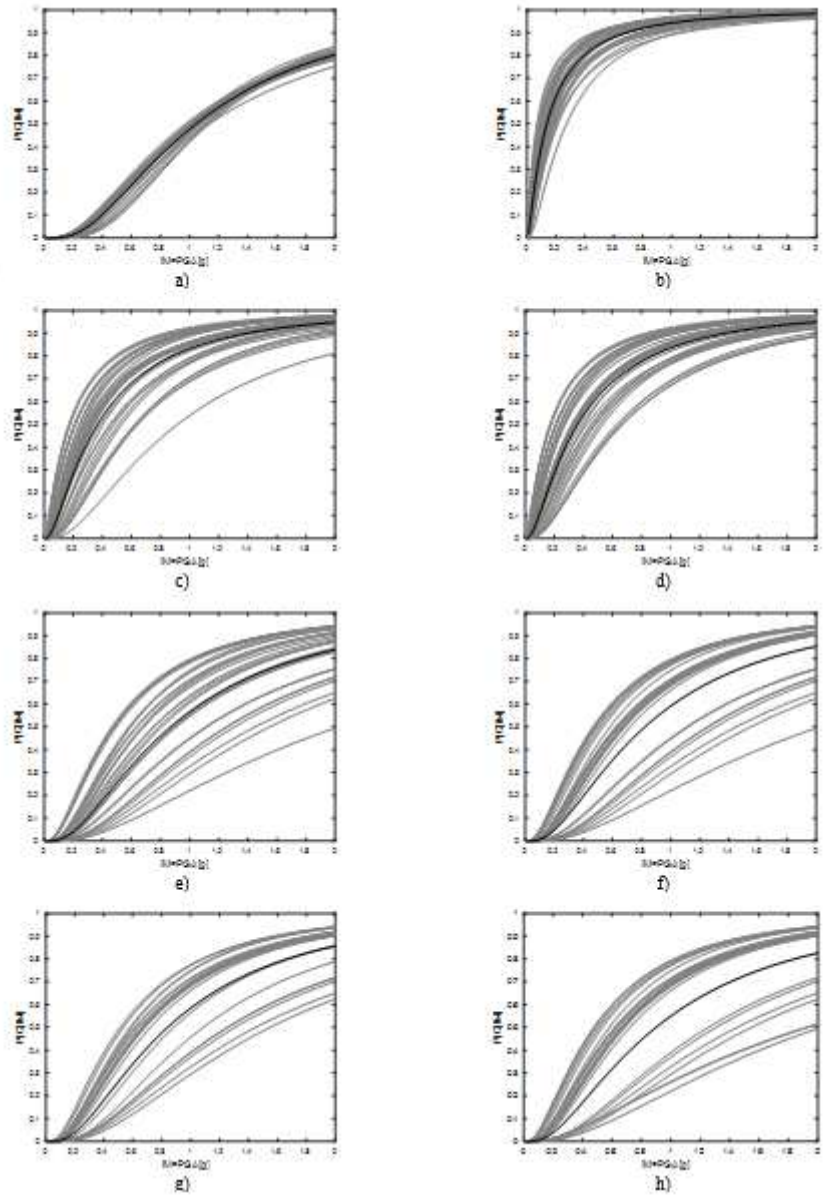

Figure 15

fragility curves from CARTIS database: a) top floor vertical bending, b) overturning of the first floor, c) overturning of two floors for MUR1, d) overturning of two floors for MUR2 class, e) overturning of three floors for MUR1 class f) overturning of three floors for MUR2 class, g) overturning of four floors for MUR1 class, h) overturning of four floors for MUR2 class

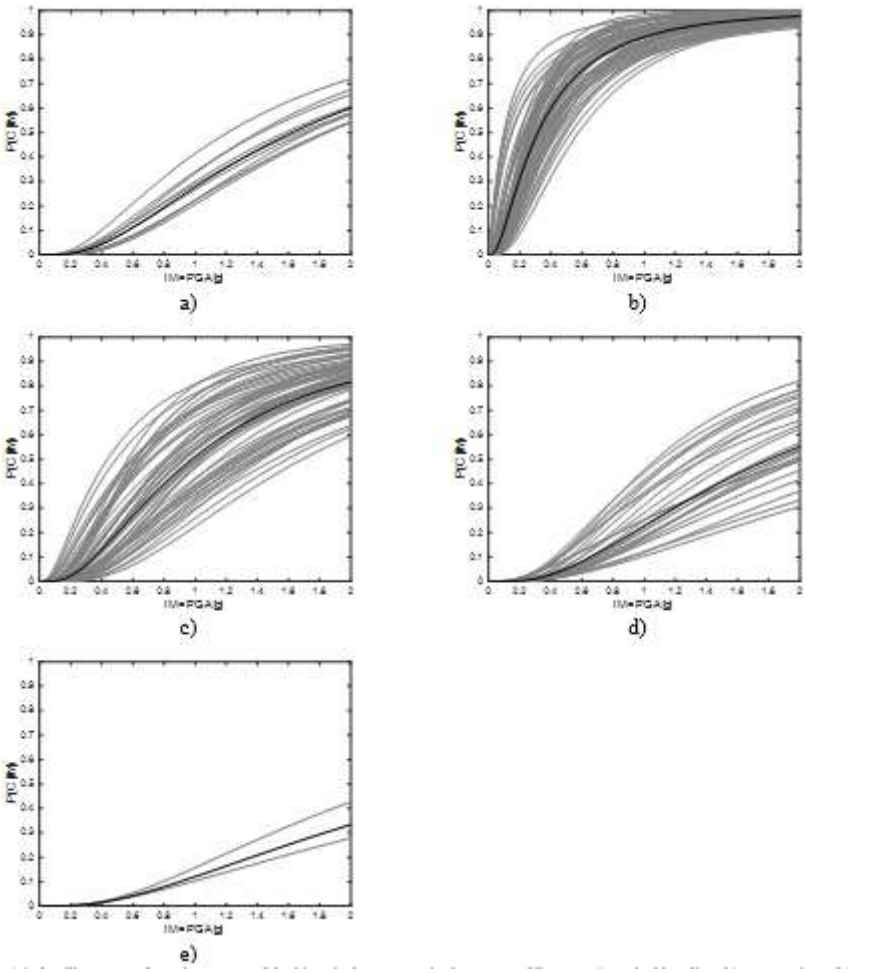

Figure 16

fragility curves from the survey of the historical aggregate in the center of Ferrara: a) vertical bending, b) overturning of the first floor, c) overturning of two floors, e) overturning of three floors

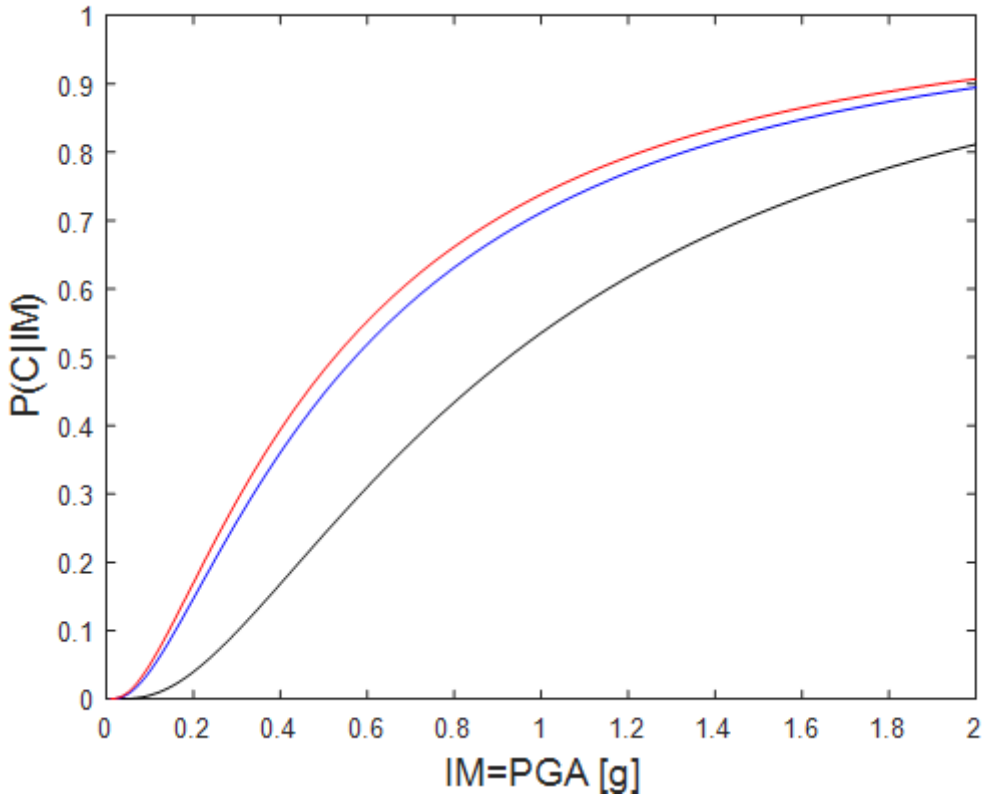

Figure 17

comparison between the average curves obtained from the population created from the Cartis database and the average curves obtained from the survey of the historical aggregate: difference between the typological survey curve (back line), the typological curve MUR1 (blue line) and the typological curve MUR2 (red line)